Spatio-temporal variations of water sources and mixing spots in a riparian zone

Guilherme E. H. Nogueira[1]; Christian Schmidt [2]; Daniel Partington [3]; Philip Brunner [4]; Jan H. Fleckenstein[1,5]

5   [1] Department of Hydrogeology, Helmholtz-Centre for Environmental Research - UFZ, Leipzig, Germany.

[2] Department of Aquatic Ecosystem Analysis, Helmholtz-Centre for Environmental Research - UFZ, Magdeburg, Germany.

[3] National Centre for Groundwater Research and Training, & College of Science and Engineering, Flinders University, Adelaide, Australia.

10   [4] Centre for Hydrogeology and Geothermics, University of Neuchâtel, Neuchâtel, Switzerland.

[5] Bayreuth Centre of Ecology and Environmental Research, University of Bayreuth, Bayreuth, Germany.

Correspondence to: Guilherme E. H. Nogueira (*guilherme.nogueira@ufz.de*)

Abstract. Riparian zones are known to modulate water quality in stream-corridors. They can act as buffers for
15   groundwater borne solutes before they enter the stream at harmful, high concentrations, or facilitate solute turnover and attenuation in zones where stream water (SW) and groundwater (GW) mix. This natural attenuation capacity is strongly controlled by the dynamic exchange of water and solutes between the stream and the adjoining aquifer, creating potential for mixing-dependent reactions to take place. Here, we couple a previously calibrated transient and fully-integrated 3D surface-subsurface, numerical flow model with a Hydraulic Mixing Cell (HMC) method to map
20   the source composition of water along a reach of the 4th-order Selke stream and track its spatio-temporal evolution. This allows us to define zones in the aquifer with similar fractions of surface- and groundwater per aquifer volume (called "mixing hot-spots"), which have a high potential to facilitate mixing-dependent reactions and in turn enhance solute turnover. We further evaluated the HMC results against hydrochemical monitoring data. Our results show that on average about 50% of the water in the aquifer consists of infiltrating SW. Within about 200m around the stream
25   the aquifer is almost entirely made up of infiltrated SW with nearly no other water sources mixed in. On average, about 9% of the aquifer volume could be characterized as "mixing hot-spots", but this percentage could rise to values nearly 1.5 times higher following large discharge events. Moreover, event intensity (magnitude of peak flow) was found to be more important for the increase of mixing than event duration. Our modelling results further suggest that discharge events more significantly increase mixing potential at greater distances from the stream. In contrast near the
30   stream, the rapid increase of SW influx shifts the ratio between the water fractions to SW, reducing the potential for mixing and the associated reactions. With this easy-to-transfer framework we seek to show the applicability of the HMC method as a complementary approach for the identification of mixing hot-spots in stream corridors, while showing the spatio-temporal controls of the SW-GW mixing process and the implications for riparian biogeochemistry and mixing-dependent turnover processes.

35

1 Introduction

1.1 Importance of mixing at the riparian zone

40 The importance of riparian zones for regulating water quality in stream corridors has long been recognized (Bernhardt et al., 2017; Gu et al., 2012; Hill, 1996; Jencso et al., 2010; Mayer et al., 2006; McClain et al., 2003; Vidon et al., 2010). Their natural attenuation capacity is partly related to dynamic water and solute exchanges between the stream and aquifer. Specifically, the mixing of stream water (SW) and groundwater (GW) within the riparian zone increases the potential for biogeochemical reactions by bringing different reactants in contact (Gassen et al., 2017; Hester et al.,

45 2014, 2019; Sawyer, 2015; Sawyer et al., 2014; Trauth et al., 2015). For instance, riparian zones have shown large removal capacities for nitrate (NO_3^-) derived from nitrogen-based fertilizers leaking into groundwater below agricultural areas (Ocampo et al., 2006; Pinay et al., 2015; Ranalli and Macalady, 2010; Vidon and Hill, 2004). Particularly along losing stream sections, infiltrating SW can increase the availability of dissolved organic carbon (DOC) as an electron donor in the riparian aquifer and in turn enhance denitrification rates following oxygen depletion

50 (Battin, 1999; Trauth et al., 2018; Zarnetske et al., 2011).

The transit of a stream water parcel after infiltration across the streambed into the riparian aquifer is followed by progressive mixing with ambient groundwater. Here, we refer to mixing at the macroscopic level, i.e. the colocation of different source waters within a defined volume of the aquifer (e.g. a numerical model cell or element), rather than pore-scale, physical-mixing, which leads to solute molecules being present simultaneously in an overlapping area

55 (Bear and Verruijt, 1987; Cirpka and Kitanidis, 2000; Dentz et al., 2011; Kitanidis, 1994). Increased macroscopic mixing, however, will in turn also lead to increased potential for physical mixing and associated reactions. In this sense, several studies have showed how macroscopic SW-GW mixing dynamics can control biogeochemical reactions within the riparian zone (Hester et al., 2013; McClain et al., 2003; Sawyer, 2015; Sawyer et al., 2014; Sawyer and Cardenas, 2009; Song et al., 2018; Stegen et al., 2016). For example, Hester et al. (2019) have demonstrated that

60 increasing stream stage enhanced the mixing-dependent denitrification of upwelling NO_3^-, with a concomitant shift of the SW-GW mixing-interface to deeper parts of the hyporheic zone (HZ). Moreover, it has been proven that the highest potential for mixing-dependent turnover of groundwater-borne solutes is at the fringe of the HZ, where mixing between infiltrating SW and local flowing GW might develop to a larger degree (Hester et al., 2014, 2017, 2019; Sawyer and Cardenas, 2009; Trauth et al., 2015; Triska et al., 1989), Fig.1. These mixing-triggered processes could

65 represent the last natural protection before harmful groundwater-borne solutes such as NO_3^- enter a stream. As SW-GW exchange (and subsequent SW-GW mixing) is a spatially and temporally dynamic process, identifying the different water sources within the riparian zone and their mixing dynamics can be helpful to advise adequate stream restoration plans to improve aquatic ecosystem health (Hester et al., 2017; Lawrence et al., 2013). However, to the best of our knowledge, the continuous spatio-temporal changes of SW-GW mixing degrees due to transient

70 hydrological forces have rarely been assessed at the stream corridor scale (Berezowski et al., 2019; Gomez-Velez et al., 2017; Lessels et al., 2016; Liggett et al., 2015). This is partly due to the significant effort required to identify different water sources and their dynamics at high spatio-temporal resolution at the river corridor scale.
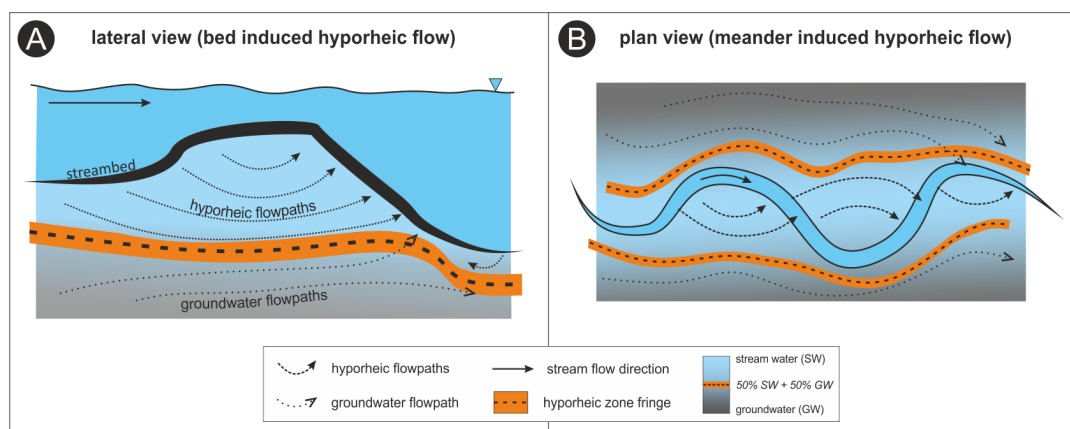
Fig.1: Scheme of two different hyporheic flow types and their flow paths. The orange area highlights the hyporheic zone fringe (Triska *et al.*, 1989), with highest turnover potential for groundwater-borne solutes.

75

1.2 Identification of water sources and their relative abundance in the riparian zone.

In order to map different water sources and assess the locations and temporal variations of SW-GW exchange processes at different scales within stream corridors, end-member mixing models (e.g., with Chloride, or other

80 traceable chemical components or isotopes) have been used. They can reveal spatio-temporal patterns of mixing in the riparian zone and provide a quantitative estimate of mixing ratios (Appelo and Postma, 2005; Battin, 1999; Pinay et al., 1998; Schilling et al., 2017; Stigter et al., 1998), as long as it is possible to properly identify the system end-members (McCallum et al., 2010). Geostatistical methods have also been used to identify and understand the distribution of different water sources within riparian zones (Lessels et al., 2016). However, these approaches rely on

85 intense water sampling for identifying the extent, to which different water sources mix (Biehler et al., 2020; Lessels et al., 2016; Schneider et al., 2011). Yet, such methods still have limitations in capturing the full spatio-temporal dynamics of SW-GW exchange and mixing in stream corridors. Assessing the spatio-temporal evolution of mixing zones and their implications for the biogeochemistry of stream corridors remains a significant challenge.

The use of hydrodynamic models can yield detailed insights into stream-riparian zone exchange dynamics (Broecker

90 et al., 2021; Hester et al., 2017; Liu and Chui, 2018). In particular 3D fully-integrated surface-subsurface models that explicitly account for SW-GW exchange fluxes at high spatial and temporal resolution, such as HydroGeoSphere (HGS, Aquanty Inc., 2015) or ParFlow (Kollet and Maxwell, 2006) are well suited for this purpose. Still, most numerical models cannot quantify the extent of different water sources solely based on computed water fluxes and resulting water flow paths (Gomez-Velez et al., 2017). Such quantification usually requires additional solute transport

95 routines, and in turn extra computational resources. The Hydraulic Mixing-Cell (HMC) method (Partington et al., 2011) is one such approach that allows a quantification of mixing and can be applied to any hydrological model that provides an explicit fluid mass balance at sufficiently resolved spatial scale (e.g., at the scale of numerical model cells). The method was originally developed to identify the contribution of different water sources - namely surface

water (e.g., surface runoff) and groundwater - to the total streamflow hydrograph (Gutiérrez-Jurado et al., 2019;
100 Liggett et al., 2015; Partington et al., 2012, 2013), but it has also been applied to track water from different sources in
other contexts such as groundwater abstraction (Schilling et al., 2017), or the spatio-temporal variation of mixing
fronts (Berezowski et al., 2019).

1.3 Purpose of this study

105 In this study, we aim to map the different water sources and assess the dynamics of their macroscopic mixing within
a riparian zone in order to evaluate the potential for biogeochemical turnover. To do so we use a state of the art
numerical model and mixing cell routine. Rather than explicitly simulating the reactions induced by SW-GW mixing
(Hester et al., 2014, 2019), our objectives are to:

1. quantify the different water sources within the riparian zone and their spatio-temporal evolution;
110 2. assess the relationship between flow dynamics and the degree of macroscopic mixing of these different waters; and
3. evaluate the formation and dynamics of mixing hot-spots within the riparian zone.

To reach our objectives we do not aim to produce a meticulously calibrated, complex model for the studied site, but
rather to harness the insights that detailed field observations in conjunction with such numerical modelling of
115 macroscopic mixing provide (i.e., an "hypothetical reality") (Mirus et al., 2011). We again emphasize that here
"mixing" refers to the colocation of different source waters within a defined volume of aquifer (e.g., a numerical
model cell). Mixing degrees were computed based on transient results of HMC, which does not require further solute
transport simulations in order to track different water components in space and time. The HMC routine was coupled
to a transient and fully-integrated 3D numerical flow model covering the riparian zone of a 4th-order stream. We
120 evaluate the HMC results in the light of hydrochemical data, and further quantify distinct mixing hot-spots that have
the potential to enhance mixing-dependent turnover processes (Hester et al., 2014, 2019; Trauth et al., 2014). With
this easy-to-transfer framework we also seek to demonstrate the utility of the HMC method for the identification of
mixing hot-spots at the river-corridor scale.

2 Methods
125

The steps followed in this study to assess the spatio-temporal variations of water sources and mixing within a riparian
zone are summarized in Fig.2.
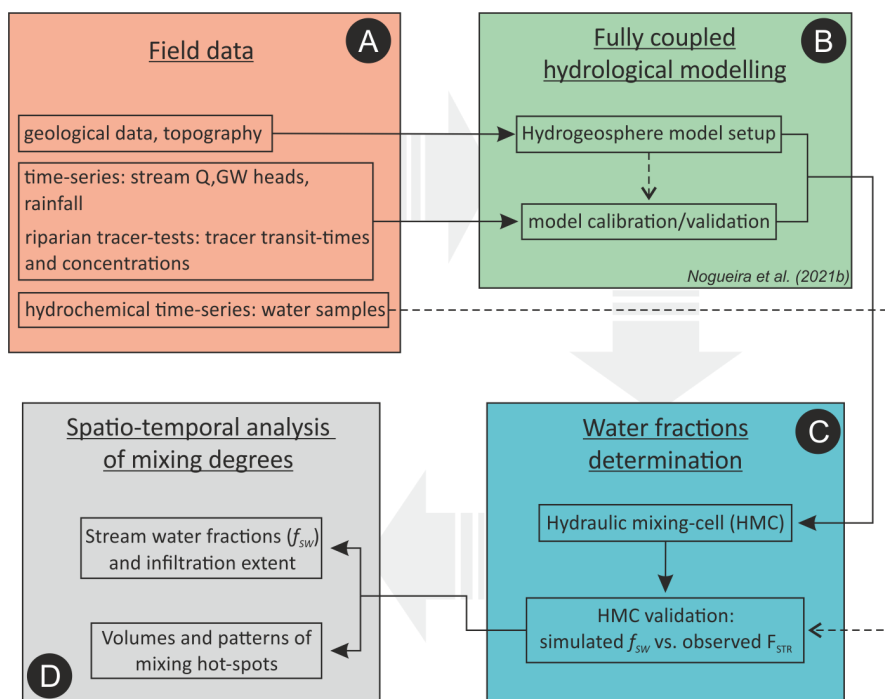
Fig.2: Flowchart of methods used to assess the spatio-temporal dynamics of the hyporheic zone and of the mixing degrees.

130

2.1 Study area and hydrological modelling

We coupled the HMC method to a previously calibrated numerical surface-subsurface flow model (Nogueira *et al.,* in press) of a highly instrumented test-site of the TERENO observatory (Wollschläger et al., 2017). The study site is located within the catchment of the Selke Stream, a 4th-order perennial stream, in central Germany, Fig.3. The studied

135 stream section (appx. 900 m) is characterized by predominantly losing conditions, which has been linked to enhanced turnover of groundwater-borne NO_3^- at the site due to mixing with infiltrating stream-borne DOC and subsequent denitrification (Gassen et al., 2017; Lutz et al., 2020; Trauth et al., 2018). The alluvial aquifer consists of up to 8 m-thick fluvial sediments, with grain sizes ranging from medium sands to coarse gravels, underlain by less permeable clay-silt deposits forming its bottom. The numerical flow model presented in Nogueira *et al.,* in press, which is based

140 on the code HydroGeoSphere (HGS), is used here for coupling the HMC method since HGS explicitly computes fluid mass balances at every model cell and in each time-step of the simulation. HGS provides a fully-integrated 3D solution for variably saturated subsurface flow (using Richards's equation) and a 2D depth-averaged solution for surface flows based on the diffusive wave approximation to the St. Venant equations (Therrien et al., 2010).
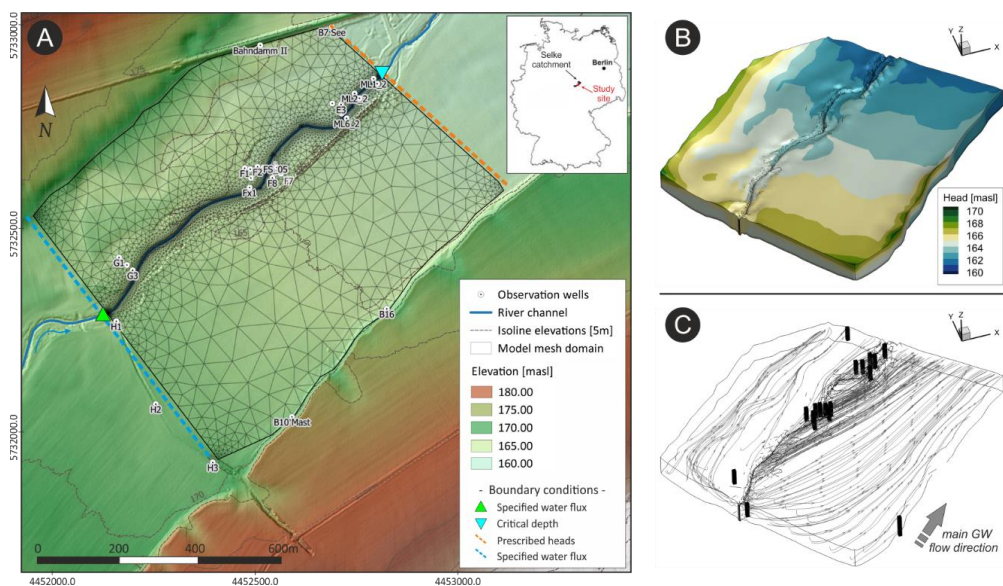
145   **Fig.3: a)** study area and model domain; **b)** simulated groundwater heads for a baseflow (Q=0.1 m³/s) scenario; **c)** streamlines (grey lines) depicting main groundwater flow direction for the baseflow scenario. Black vertical lines in (c) depict some of the wells shown in (a). Note the vertical exaggeration of the 3D plots (10x).

The flow model parameterization is only briefly summarized here, as the model and its calibration are described in
150   detail in Nogueira *et al.* (in press). The model was calibrated using the PEST software (Doherty, 2018) based on
stream discharge values, multi-well groundwater heads, as well as multiple breakthrough curves from performed
groundwater tracer-tests (Nogueira et al., 2021a, in press). Automatically calibrated parameters were within the
literature ranges and the calibrated model showed a very good match between observed and simulated values, with
coefficient of determination (R²) and Kling-Gupta-Efficiency (KGE) (Gupta et al., 2009; Knoben et al., 2019)
155   generally above 0.8 and 0.5, respectively. The flow model was calibrated for the period of 2017-2018 and here we
have only implemented changes in the boundary conditions (BCs), without any additional model calibration. We
performed transient simulations using daily forcing inputs for the hydrological years 2013-2016 since this is the period
with more hydrochemical data available to further validate the HMC results. The BCs on the model surface domain
were defined as (i) groundwater recharge (as a fraction of daily precipitation) at the model top, (ii) specified water
160   flux at the model stream inlet according to discharge values measured at a gauge station about 3000m upstream of
the study site, and (iii) a critical depth BC at the model stream outlet (Fig.3a). The BCs on the subsurface model
domain were defined as (iv) specified water flux representing ambient groundwater flow at the upstream side of the
model, and (v) prescribed time-varying hydraulic heads at the downstream side of the model, Fig.3a. The quality of
the flow model was evaluated according to the water balance error, R² between observed and simulated groundwater
165   heads and stream discharge, as well as KGE.

2.2 The Hydraulic Mixing-Cell (HMC) method

The contribution of water sources (and subsequent mixing degrees) in each model cell was calculated with the HMC method (Partington et al., 2011, 2012, 2013). The different water sources have to be predefined in terms of their origin (e.g., stream water, groundwater, and rainfall), which are related to the BCs applied to the numerical model. HMC calculation depends only on computed nodal water fluxes and does not involve any extra parameters. The HMC method uses the ''modified mixing rule'', which simulates a mixing regime between perfect mixing and piston flow. Initially, all model cells have an artificial "initial" water fraction. In the subsequent time-steps, different water sources are mixed according to volumes of water flowing into and out of a cell accordingly (Partington et al., 2011):

$$f_{i(w)}^t = \left(\frac{V_i^{t-1}}{V_i^t} - \frac{Vbc_{out}^t + \sum_{j=1}^{m} V_{ij}|_{t-1}^t}{V_i^t} \right) f_{j(w)}^{t-1} + \frac{Vbc_k^t + \sum_{j=1}^{n} V_{ji}|_{t-1}^t \; f_{j(w)}^{t-1}}{V_i^t} \qquad (1)$$

where $f_{i(w)}^t$ [-] is the computed water fraction w at time-step t in cell i, n and m are sources and sinks for cell i, $f_{j(w)}^{t-1}$ denotes the water fraction w at time $t\text{-}1$ in a neighbouring cell j, V denotes the volume with the superscript denoting time-step and subscript i denoting the cell, ij denoting volume into cell j from cell i over the time-step from $t\text{-}1$ to t, ji denoting volume from neighbour cell j into cell i, and Vbc_w^t is a volume from the inflowing boundary condition associated with water fraction w and Vbc_{out}^t is a volume summed from all outflowing boundary conditions at cell i. Inflow from adjacent cells is assigned the computed water fractions from the upstream cell. The HMC has an independent sub-time-step routine to calculate water fractions between the adaptive HGS time-steps, which circumvents the need of extremely small time-steps in the HGS simulations (Partington et al., 2013). This sub-routine is required to avoid instability during the HMC calculations, which can occur if the volume of water leaving a cell over a time-step is greater than the volume in storage.

Within our simulations, we defined three main water sources to be tracked, namely stream water (f_{SW}), groundwater (f_{GW}), and floodplain water (f_{FW}). The f_{SW} represents any water parcel that infiltrates into the subsurface domain through streambed cells; the f_{GW} represents groundwater flowing into the domain through the upstream subsurface boundary; the f_{FW} represents water that percolates from soil top through the unsaturated zone (e.g., from rain or flood events). An additional water source named initial groundwater (f_{GWi}) was defined representing the "initial" water residing in the model cells at the beginning of the simulations. We carried out a warm-up period during the simulations in order to flush f_{GWi} and have a more realistic distribution of the three water fractions at the domain at the start of our analyses. The warm-up period consisted of a two-year simulation period using constant average BC values.

The sum of all HMC fractions in each model cell is [$f_{SW}+f_{GW}+f_{FW}+f_{GWi}$]=1, for an error-free fluid mass balance. With that approach, we can evaluate the composition of the different water fractions at any time-step and location at the model domain. We further spatially aggregated the different HMC fractions to assess the temporal variation of their contribution to the total volume of the simulated domain with the *Integration* function in TecPlot 360 EX, Version 2019 R1 (TecPlot, Inc.) using the different HMC fractions as scalar variables and dividing the results by the total volume of the simulated domain:

$$V_w = \frac{\sum_{p=1}^{P} f_w}{V_{tot}} \times 100\% \tag{2}$$

200   where V_w is the total volume of a HMC fraction w in a given time-step, p is a cell (from 1 to P) with a specific water

fraction f_w (e.g., f_{SW}, f_{GW}, f_{FW}), and V_{tot} is the total volume of the simulated domain (4.63×10^6 m³).

A similar version of Eq.2 was used to assess the spatio-temporal evolution of the hyporheic zone (HZ). To do so, we

employ the *geochemical definition* of the HZ, similar to the one proposed by Triska et al. (1989), where the HZ is the

area within the riparian zone containing more than 50% stream water ($f_{SW} \geq 0.5$) in the mixture of waters. Using Eq.2,

205   we computed the total volume of the HZ (V_{HZ}) in each time-step by only aggregating cells presenting $f_{SW} \geq 0.5$ in the

domain. This *geochemical definition* was preferred over the *hydrodynamic definition* (Gooseff, 2010; Trauth et al.,

2013) because of its stronger relevance for biogeochemical transformations (Boano et al., 2010; Gomez-Velez et al.,

2017). Besides, in strongly losing streams, the HZ definition based on hyporheic streamlines (i.e., *hydrodynamic

definition*) would describe the HZ as a very narrow zone limited to the streambed and its immediate vicinity only,

210   since most of the infiltrating SW does not immediately return to the stream.

2.3   HMC validation and stream water fraction calculation

In order to validate the HMC results, we compared the simulated stream water fractions (f_{SW}) with the calculated

stream water fractions (F_{STR}) at riparian observation wells. The F_{STR} is based on a two end-member chloride (Cl⁻)

215   linear mixing model (Appelo and Postma, 2005). By assuming Cl⁻ as a conservative solute, mixing between two

independent end-members occurs, namely stream water and groundwater farther away from the stream (not affected

by infiltrating stream water). The fraction of stream water in the riparian groundwater was computed as:

$$F_{STR} = \frac{[Cl^-_{obs}] - [Cl^-_{GW}]}{[Cl^-_{SW}] - [Cl^-_{GW}]} \tag{3}$$

where $[Cl^-_{obs}]$, $[Cl^-_{GW}]$, and $[Cl^-_{SW}]$ indicates the Cl⁻ concentration measured in an observation well, in the groundwater

220   distant from the stream, and in the stream at a given time, respectively. Calculations and measurements are based on

biweekly collected water samples of 2014-2016. Groundwater was sampled with a peristaltic pump placed at the

middle of the fully screened wells and surface water was collected as grab samples. Samples were stored and analysed

in the lab following standard procedures (Trauth et al., 2018). The groundwater end-member $[Cl^-_{GW}]$ was assumed to

be equal to values from the observation well B10 (95 ± 5 mg L⁻¹, Fig.S1, supplementary material). To compare F_{STR}

225   and f_{SW}, we extracted simulated f_{SW} values from the locations of the observation wells in the numerical model by

averaging the f_{SW} values of all fully-saturated cells that comprises each well position. That was done to approximate

how water samples were collected at the fully screened wells, which likely results in sampling of a mix of the whole

saturated column rather than from a specific groundwater depth. In a perfect model $F_{STR}=f_{SW}$ independent of the other

simulated HMC fractions. The quality of the results was evaluated for each well in terms of the coefficient of

230   determination (R^2) and with the nonparametric Wilcoxon rank-sum test (Ziegel et al., 2011) between F_{STR} and f_{SW}

datasets. With the test, a result of *h=0* (null hypothesis) indicates the distributions of both populations are statistically equal. A value of *h=1* (alternative hypothesis) indicates the distributions of both populations are not equal.

2.4 Calculation and analyses of mixing degrees

2.4.1 Mixing degree calculation

235   At this stage, the results enable us to track and assess the different water source compositions at different time-steps and locations of our domain. We further computed a mixing degree (*d*) to quantify the degree to which different water sources mix within a model cell (Berezowski et al., 2019). We emphasize that the quantification of mixing here does not refer to true pore-scale mixing, but it rather gives an indication of how different water sources are "mixed" within a model cell in a given time-step based on neighbouring cells inflows and outflows. In that sense it provides a proxy

240   for the potential for true pore-scale mixing to occur with that model cell.

For a three end-member mixing, where each end-member is a different water source (e.g., f_{SW}, f_{GW}, and f_{FW}), any three fractions combined could be represented by a vector in a 3D coordinate space: d=[f_{SW}, f_{GW}, f_{FW}], whereas a "perfect mixing" (e.g., equal fractions of different water sources) is represented by a vector d_p=[$^1/_3$, $^1/_3$, $^1/_3$]. Thus, the resulting mixing degree *d* can be calculated as the Euclidean distance between the vectors *d* and d_p taking into account that a

245   maximum value for a given fraction can only be 1, as well as that the fractions have to sum up to 1 within a cell (for an error-free fluid mass balance). A more general equation to quantify the mixing degree for three (or more) end-members (w) could be written as:

$$d = 1 - \left[\frac{\sqrt{\left(^1/_w - f_1\right)^2 + \left(^1/_w - f_2\right)^2 + \dots + \left(^1/_w - f_w\right)^2}}{\left(\sqrt{2} \times ^{\sqrt{w}}/_w\right)} \right] \tag{4}$$

where f_1, f_2, and f_w represent HMC fractions. For a two end-member mixing only, or in the case of a combination of

250   two end-members to a single one (e.g., f_{SW}, and [f_{GW}+ f_{FW}]), the denominator in Eq.4 would be simply ($^{\sqrt{2}}/_2$). This two end-member mixing is the preferred one used throughout the manuscript because preliminary simulations have revealed that f_{FW} is only high at the vadose zone, whereas actual volumes of percolating water from the vadose zone were proportionally very low in comparison to f_{GW} and f_{SW} at the aquifer. In this formulation, *d=1* represents a perfect mixing within a cell at a given time-step (e.g., equal water fractions: f_{SW}=0.5 and f_{GW}+f_{FW}=0.5), while smaller values

255   would indicate a disproportional contribution of one or another water sources to the mixture (e.g., too much of one water source and too few of another). By calculating *d* in every location and time-step, we can identify the model cells where the water sources of interest are mixed at equal proportions and assess its dynamics without depending on solute transport simulations.

To analyse the temporal variation of different mixing degrees, we spatially aggregated model cells presenting different

260   *d* values (e.g., *d > 0*, *d ≥ 0.25*, *d ≥ 0.50*, and *d ≥ 0.75*) in each time-step and compared them to the total volume of the simulated domain (Eq.5), as well as to the total HZ volume (Eq.6) to assess their relative percentage in each time-step:

$$V_d = \frac{\sum_{p=1}^{P} d}{V_{tot}} \times 100\% \tag{5}$$

$$V_{d\_HZ} = \frac{\sum_{p=1}^{P} d}{V_{HZ}} \times 100\% \tag{6}$$

where V_d and V_{d_HZ} are the total volume of cells presenting a certain d value within the total domain and within the
265 HZ, respectively, in a given time-step; p is a cell (from p=1 to P) presenting a certain d value; V_{HZ} is the HZ volume
according to Eq.2. Here, mixing hot-spots (d_h) are characterized by model cells presenting $d \geq 0.75$, as equally used
in Berezowski *et al.* (2019) for delineating the active perirheic zone after the definition of Mertes (1997). We also
assessed the temporal development of mixing hot-spots at the domain by comparing the peaks of d_h values from Eq.5
with the peak of discharge events observed in the simulation period. So we can evaluate when mixing-hot-spots occur
270 in relation to flow dynamics and their magnitude of occurrence. We computed the Spearman's rank correlation to rank
the metrics of discharge events (e.g., peak prominence, event duration, time-to-peak) that control the increasing in d_h.

2.4.2 Transit-times within mixing hot-spots

The development of mixing hot-spots is a good indication of the locations and moments where and when mixing-
dependent reactions such as the turnover of groundwater-borne NO_3^- due to pore-scale mixing with infiltrating SW
275 can occur. However, since time is also a relevant variable for biogeochemical processes, it is equally important to
know for how long a certain water parcel resides within mixing hot-spots. To quantify this time span, we defined
exposure-time ($d_{h-\tau}$), as the time that a water parcel resides within defined mixing hot-spots along its transit through
the riparian aquifer. We computed transit-times (τ) based on a transient particle tracking analyses according to HGS
flow model results (Nogueira et al., in press). Flow paths were extracted from each HGS time-step based on massless
280 particles released from streambed cells and from the top of the model domain. A total of around 1,300 particles were
released in each HGS time-step, capturing main groundwater flow directions and infiltrating SW flow paths.

For this analysis, we differentiated the flow paths in two categories: flow paths of SW that infiltrates and subsequently
exfiltrates back to the stream within the simulated domain (called hyporheic flow paths), and water flow paths that do
not exfiltrate to the stream within the simulated domain (called floodplain flow paths). Each flow path is divided into
285 smaller sub-sections, which were analysed in terms of HMC fractions, d_h, τ, and thus $d_{h-\tau}$. By carrying out these
combined analyses, we can assess how $d_{h-\tau}$ is affected by transient hydrological conditions. Model visualization,
integration and particle tracking analyses were performed in TecPlot 360 EX; additional calculations were carried out
with MatLab® 2019b.

290 **3 Results**

In this section we will focus on the results of simulations for the years of 2013-2016 since it was the period used for
the validation of HMC results. The results of the flow model are not detailed here, but only generalized for a better
understanding of the SW-GW exchanges dynamics and overall characteristics of the flow system. Simulated

groundwater heads and stream discharge matched the field values well, with a mean KGE of 0.73 for groundwater

295 heads and 0.84 for stream discharge (Fig.S2, supplementary material). The stream reach was characterized by predominantly losing conditions with average losses to the subsurface of around 40-50% of total discharge. This is higher than the 25% measured in the field by Schmadel *et al.* (2016) during a small discharge event in July 2014; however, our simulated losses for the same period of their analyses were around 30%.

A small gaining portion was observed for the simulated reach only at a localized deep pool downstream in the domain

300 (representing only about 1% of the total infiltrating SW), whereas the majority of infiltrating SW exited the domain via the downstream subsurface boundary. During very high discharge and overbank flow (generally $Q \geq 7.0 \text{ m}^3\text{s}^{-1}$) the near-stream riparian zone can be partially flooded. Moreover, groundwater flow paths are somewhat more parallel to the stream under low discharge and more divergent under high discharge conditions (Nogueira et al., in press).

3.1 Validation of HMC fractions

305 Before further assessment of the HMC results, the simulated stream water fractions (f_{SW}) were compared to observed stream water fractions (F_{STR}), which were calculated based on Cl$^-$ measurements for a validation of model results (Sect. 2.3). The F_{STR} computed according to Eq.2, as well as the extracted f_{SW} for some observation wells are presented in Fig.4. The locations of the wells are presented in Fig.3.
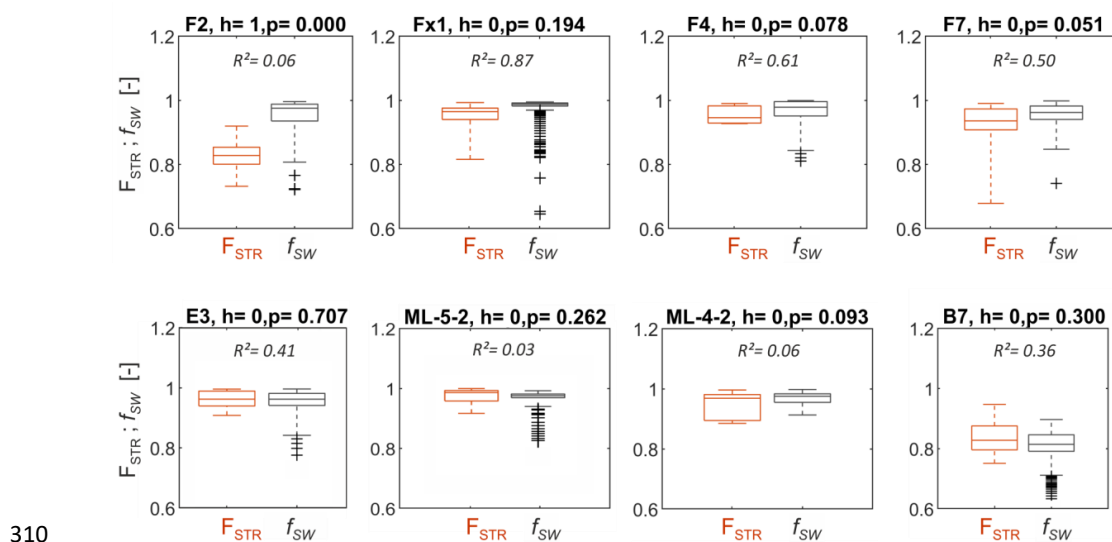
Fig.4: Observed and simulated stream water fractions (F_{STR} and f_{SW}, respectively) for some observation wells in the study area. The h values represent the results of the Wilcoxon-test between F_{STR} and f_{SW} datasets with respective *p-values* (p): h=0 indicates that the F_{STR} and f_{SW} groups are from continuous distributions with equal medians, while h=1 indicates the

difference between the medians is statistically significant; The R values show the coefficient of determination between the F_{STR} and f_{SW} datasets**. The names of the wells are shown at the top of each plot.

For 70% of all groundwater samples the mixing model was applicable for the calculation of F_{STR}. For the other samples, Cl⁻ concentrations were temporally lower than in the stream water and they were excluded from further analyses (Fig.S1, supplementary material). In general, the observation wells had exhibited high F_{STR} values, indicating higher fractions of stream water than other components like groundwater, Fig.4. Calculated F_{STR} and simulated f_{SW} for wells presented similar ranges (between 0.7 and 1.0), while F_{STR} showed slightly larger variations in comparison to f_{SW} values. Despite that, correlating calculated F_{STR} with simulated f_{SW} showed reasonable coefficients of determination (R^2 values shown in Fig.4) indicating that the model generally captures the variations of stream water fractions in the riparian groundwater for most observation wells. Small differences between F_{STR} and f_{SW} existing in some of the wells (e.g., ML wells and well F2) can be related to localized processes and conditions not captured by the model as later discussed in the manuscript. The Wilcoxon-test performed between F_{STR} and f_{SW} datasets individually for each observation well also indicated that the populations were not statistically different for the majority (indicated by h=0 on Fig.4), reinforcing the good match between simulated and observed stream water fractions on riparian groundwater.

3.2 Spatio-temporal variation of simulated HMC fractions

The temporal variation of simulated HMC water fractions (here referred to as just "fraction(s)") is presented in Fig.5. A warm-up period required to flush the initial f_{GWi} was found to be around 2 years, which is an approximation to the time required to fill the aquifer with "new" water sources. From this point on throughout the manuscript, we focus only on the analyses of the three remaining fractions (i.e., f_{SW}, f_{GW} and f_{FW}).

Integrating the different fractions over time (Eq.2), on average 35% of the simulated domain comprised water originating from the stream (f_{SW}), whereas groundwater inflowing from the upstream subsurface boundary (f_{GW}) was around 35%, and 30% consisted of water originating from the soil surface (f_{FW}). Since the HMC results indicate the water-origin rather than the water content, we further evaluate the HMC results considering only the fully-saturated portion of the model domain using Eq.2, which we can then relate to total HMC water contents in the subsurface. In terms of stream water, nearly 80% of the saturated domain presented $f_{SW} \geq 0.1$, and about 20% presented $f_{SW} \geq 0.9$. Following the geochemical HZ definition ($f_{SW} \geq 0.5$), this corresponded to around 50% of the fully-saturated domain (Fig.5b). Likewise, 50% of the fully-saturated domain consisted of surface water, followed by 40% consisting of groundwater and only 10% of floodplain water, Fig.5c. This indicates relatively small contributions of water originating from the top of the domain to the saturated portion of the aquifer for most of the simulated period.
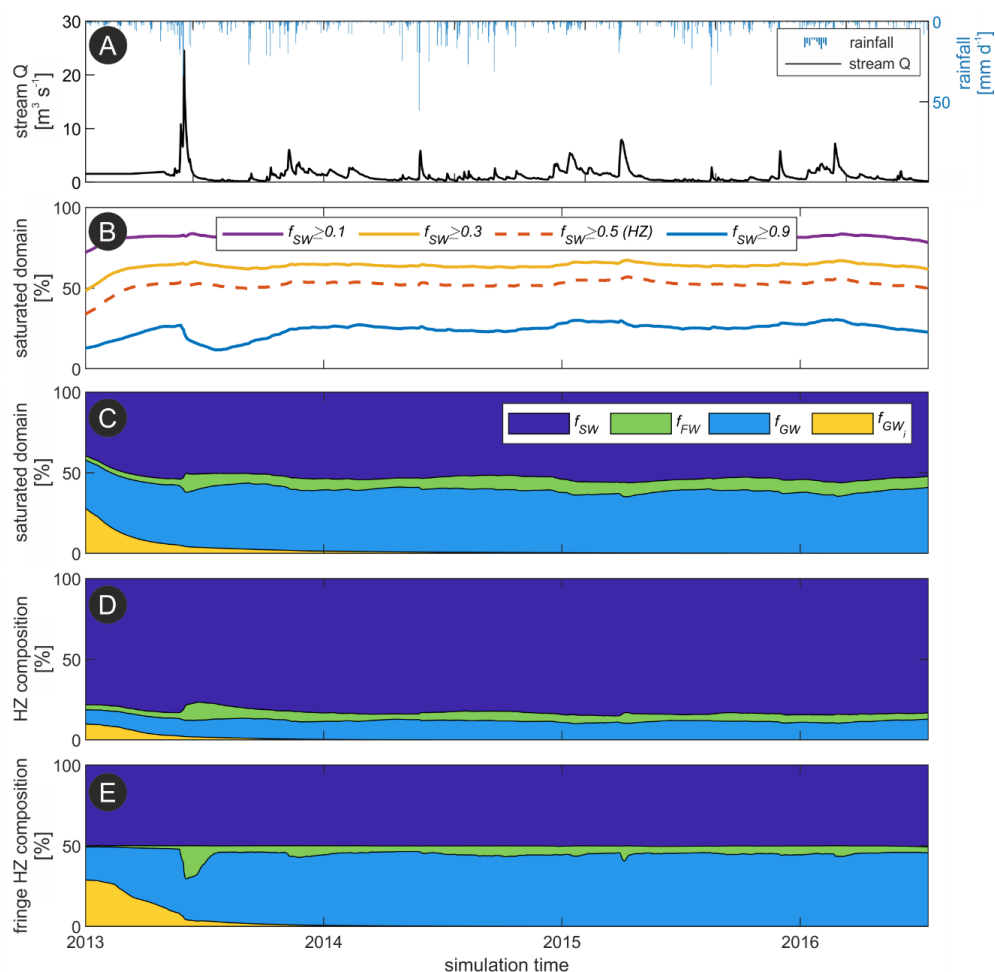
Fig.5: a) Stream discharge (Q) and rainfall time-series; **b)** temporal variation of the saturated domain consisting of at least a certain fraction (e.g., 0.1, 0.3, 0.5, and 0.9) of stream water (f_{SW}); **c)** contribution of different fractions to the saturated domain (stream water (f_{SW}), floodplain water (f_{FW}), groundwater (f_{GW}), and initial groundwater (f_{GWi})); **d)** composition of different fractions to the hyporheic zone (HZ, $f_{SW} \geq 0.5$); **e)** composition of different fractions at the fringe of the HZ ($f_{SW}=0.5$). Note that the start of the simulation (when $f_{GWi}=100\%$) is not shown in the plot.

Around 80% of the geochemical HZ volume consisted of water originating from the stream, with the rest being represented by groundwater (15%) and floodplain water (5%), Fig.5d. This already suggested that, despite the potential for subsurface biogeochemical processes and turnover of stream-borne solutes within hyporheic flow paths (Trauth et al., 2014; Zarnetske et al., 2011), there is limited potential for mixing-dependent reactions involving reactants from both water sources (SW and GW) due to the dominance of stream water in this zone. Differently, at the HZ fringe (where $f_{SW}=0.5$), f_{GW} and f_{FW} 40% and 10% respectively (Fig.5e), indicating a higher potential for mixing between the different water sources. Fig.6 shows the spatial distribution of minimum, maximum and median values, as well as

360   the standard deviation (σ) of each fraction within the domain for the entire simulation period. To better represent the maximum probable HMC water contents (and not only the proportions of the different sources) in each model cell, the fractions shown in the plot were multiplied by the maximum saturation value that was recorded in each model cell during the entire simulation period.
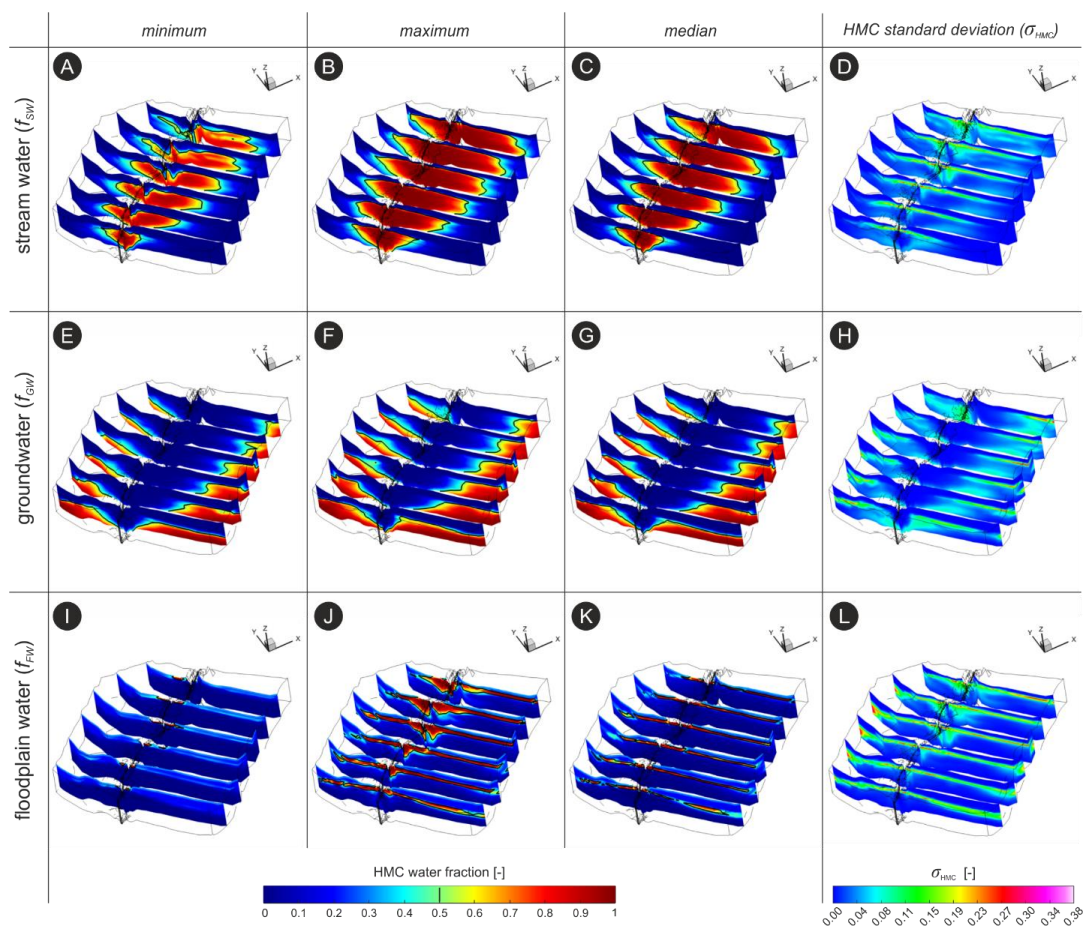
Fig.6: minimum, maximum, median values, as well as standard deviations (σ_{HMC}) of stream water (f_{SW}) **(a-d)**, groundwater (f_{GW}) **(e-h)**, and floodplain water (f_{FW}) **(i-l)** fractions for the entire simulation period. The black line **(a-c, e-g, i-k)** indicates the HMC fractions of 0.5. Note the vertical exaggeration of the 3D plots (20x).

370   Throughout the simulation, f_{SW} was high around the stream and decreased with distance from the stream, Fig.6a-c, reaching values of 0.5 at around 150-200m from the stream channel, which defines the local geochemical HZ. This regularity was maintained by the continuous SW infiltration to the aquifer due to the overall losing conditions of the stream reach. The f_{SW} plume was slightly smaller at upstream areas due to boundary condition effects. There was also

a large variation of f_{SW} values around the stream and at the groundwater-table interface (Fig.6d). High values of f_{GW}

375 were only observed at the periphery of the simulated domain, as well as at the southern upstream face of the domain (boundary effect), Fig.6e-g. Lastly, high f_{FW} values were mainly observed above the groundwater-table. However, since absolute water content (i.e., saturation) is low at these areas, the total f_{FW} content is also relatively low in comparison to other HMC fractions, Fig.6i-k. Still, some high f_{FW} values were recorded in the subsurface (Fig.6j), when a considerable volume of water originating from the stream flows overbank and subsequently percolates through

380 the riparian soils (e.g., following the high discharge event on Jun-2013, Fig.S3, supplementary material). Although the model indicates this is floodplain water, it is important to keep in mind that it is overbank flow of stream water that subsequently percolates into the subsurface after flooding.

3.3 Spatial variation of mixing degrees

385 Despite the nearly constant spatial distribution of fractions throughout the domain (Fig.6), flow dynamics and stream stage fluctuations resulted in different mixing degrees between the different fractions. The plots in Fig.7 show the spatial distribution of minimum, maximum and the median values of mixing degree, as well as its standard deviations (σ_d) for the entire simulation period (2013-2016).
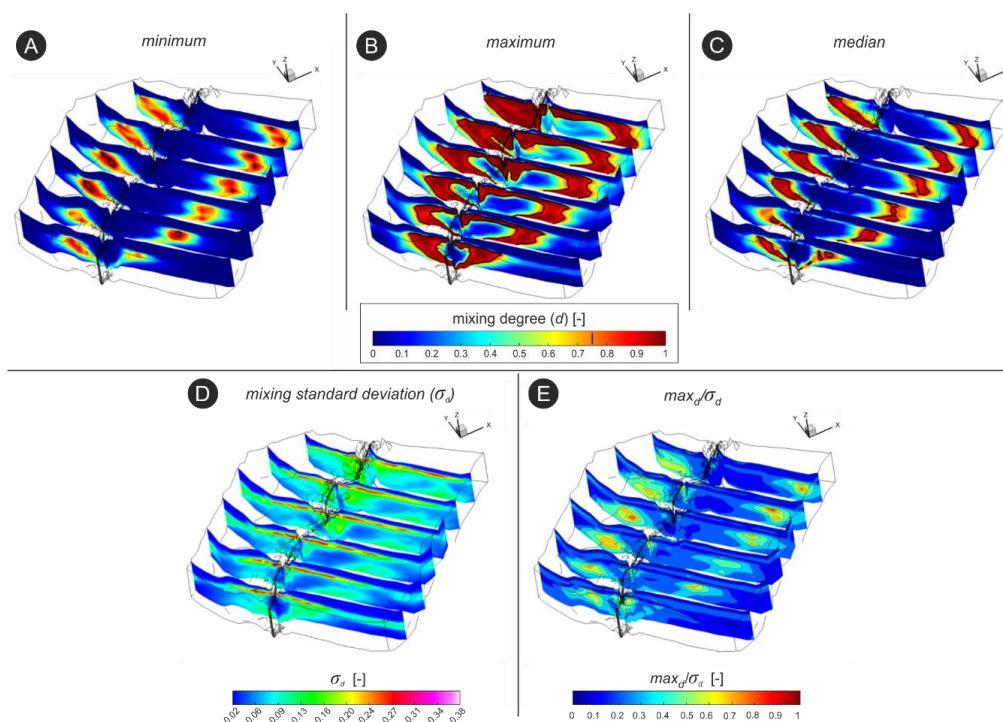
390   **Fig.7:** minimum **(a)**, maximum **(b)**, median **(c)**, standard deviation (σ_d) **(d)**, and the normalized ratio $\max_d/\sigma_d$ **(e)** for mixing

degrees for the entire simulation period. The black lines **(a-c)** indicate regions with *d=0.75* (*mixing hot-spots*, d_h). Note the

vertical exaggeration of the 3D plots (20x).

The relatively high f_{SW} within the HZ prevents high mixing degrees to occur near the stream. In contrast, regions at

395   the fringe of the HZ presented the highest minimum *d* values over the entire simulation period (Fig.7a), which suggest

constant high *d* values in those areas. Yet, larger *d* values also occurred near the stream at some points during the

simulation (Fig.7b). These large *d* values near the stream followed discharge events with partial flooding of the riparian

zone, which leads to large percolation of inundation water into the riparian aquifer, which then mixes with infiltrating

SW and with ambient groundwater. Nevertheless, the computed median values of *d* indicate that *mixing hot-spots* (d_h)

400   ($d \geq 0.75$) were indeed more persistent near the HZ fringe (Fig.7c). In comparison to regions near the groundwater-

table interface, for example, these areas at the HZ fringe also presented slightly smaller σ_d (Fig.7d), showing smaller

variation in time. We further quantified the persistence of *mixing hot-spots* in time by computing and normalizing the

ratio of maximum *d* over their σ_d ($\max_d/\sigma_d$) since a small σ_d alone does not imply a persistent *mixing hot-spot* over

time. A high value of this metric would indicate the occurrence and persistence of *mixing hot-spots* over the entire

405   simulation period, as it can be observed near the HZ fringe for instance (Fig.7e) where $\max_d/\sigma_d$ are generally above

0.5. These areas comprise only around 5% of the total model domain.

3.4   Temporal variation of mixing degrees

Mixing degrees also varied in time, as could be concluded from the plots in Fig.7. Here, we further assessed how

mixing degrees varied over time, as well as their relationship with flow dynamics. For that, we have integrated cells

410   with at least a certain degree of mixing (e.g., *d > 0*, *d ≥ 0.25*, *d ≥ 0.50*, and *d ≥ 0.75*) and compared them to the total

volume of the domain (Eq.5). Around 80% of the domain presented some sort of mixing (*d > 0*), which strongly varied

over time suggesting the activation of areas that do not present consistent mixing throughout the simulation, Fig.8b.

Zones with *d ≥ 0.25* were on average 40% of the total domain. Only around 9% of the total domain presented *d ≥ 0.50*,

which was just slightly larger than d_h (*d ≥ 0.75*). Moreover, d_h represented 7-12% of the total domain volume (Fig.8c).

415   In relation to the geochemical HZ, *mixing hot-spots* were comparatively higher and represented on average 23%

(between 15% and 30%) of the total HZ volume (Fig.8d).
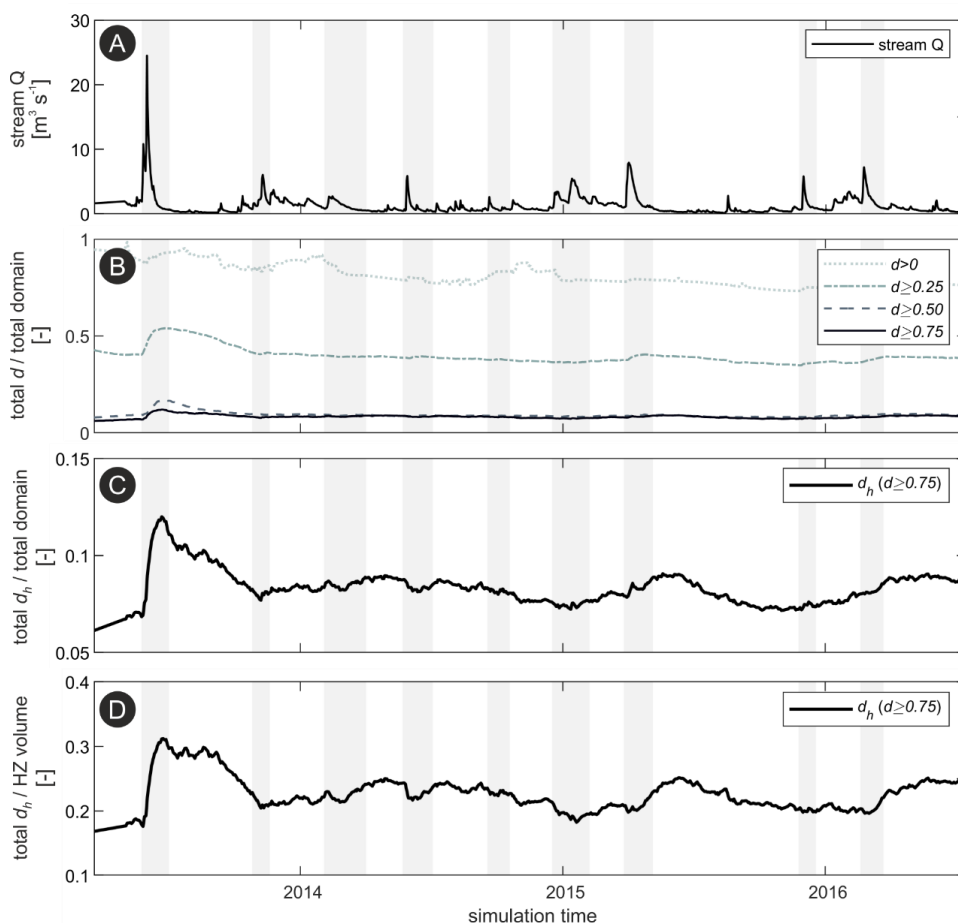
Fig.8: a) time-series of stream discharge for the period of 2013-2016; **b)** total volume of cells presenting a certain degree of

420   mixing ($d>0$, $d≥0.25$, $d≥0.50$, and $d≥0.75$) in relation to total domain volume; **c)** total volume of mixing hot-spots (d_h, $d≥0.75$) in

relation to total domain volume; and **d)** total volume of d_h in relation to total hyporheic zone (HZ) volume. Grey vertical bars

indicate discharge events periods.

The impacts of discharge (Q) variations on d were also evident (Fig.8b). Concerning *mixing hot-spots*, discharge

425   events increased d_h by 5-10% in comparison to conditions immediately before the start of the events (Fig.8c).

Spearman's rank correlation (Table 1) showed that the discharge peak prominence (ΔQ) (in relation to Q value prior

to the event) and the increase of d_h from the value immediately prior the event ($Δd_h$) were positively correlated

(R_{spear}=0.96). Both the event duration and the time-to-peak were not strongly correlated to $Δd_h$ (R_{spear}=0.09 and

R_{spear}=0.30, respectively) (Fig.S4, supplementary material). In our simulations, event duration and peak prominence

430   were also not strongly correlated (R_{spear}=0.14, data not shown).

Moreover, the lag between the peak of the discharge events and the peak of d_h was 14 days on average, somewhat shorter for events presenting higher ΔQ, but the metrics showed only a weak correlation ($R_{spear}=0.28$). On the other hand, event duration and the lag between the peak of the discharge events and the peak of d_h showed a good correlation ($R_{spear}=0.66$), suggesting that longer events would lead to later developments of d_h. Due to the temporal lag between

435   the peak of Q events and peak of d_h, mixing degrees were generally higher during the recession of discharge events.

Table 1: Overall Spearman's rank correlation between metrics of discharge events and the increasing of mixing hot-spots (d_h) at the riparian zone.

Discharge events metrics	Correlation to Δd_h
Event duration [days]	0.009
Time-to-peak [days]	0.305
Time-to-peak/event duration [-]	0.340
Peak prominence (ΔQ) [m³ s⁻¹]	0.963

Lag between Q *peak-event* and following peak d_h [days]	
Min	1
Mean	14
Max	46

R_{spear} between ΔQ and lag to peak d_h: 0.28
R_{spear} between event duration and lag to peak d_h: 0.66

3.5   Exposure-times ($d_{h\text{-}\tau}$)

Since the time that a water parcel resides within *mixing hot-spots* also affects the potential for biogeochemical
440   processes, for each flow path we computed exposure-time ($d_{h\text{-}\tau}$), as the share of water transit-times (τ) spent within *mixing hot-spots*. Overall, $d_{h\text{-}\tau}$ were generally smaller during the peak of discharge events since: i) groundwater velocities are higher during events, leading to relatively shorter τ (Fig.9a), and ii) d_h was relatively smaller during peak events (Fig.8c). Since transit-times are generally longer under baseflow conditions (Fig.S5, supplementary material), $d_{h\text{-}\tau}$ was equally longer during the recession of discharge events (Fig.9b).

445   Specifically, the median $d_{h\text{-}\tau}$ of floodplain flow paths (i.e., water parcels that do not exfiltrate through streambed cells within the model domain) was highly variable in time (3-12 days), on average 15% of the total flow path τ, Fig.9b. On the other hand, for the hyporheic flow paths (i.e., infiltrating SW that exfiltrates through streambed cells after infiltration and subsurface transit), $d_{h\text{-}\tau}$ were small (0-3 days), on average 5% of the total hyporheic τ. The median τ of floodplain flow paths were slightly stronger correlated to Q variations than hyporheic flow paths, $R_{spear}= -0.50$ and
450     $R_{spear}= -0.45$, respectively (Fig.9c).
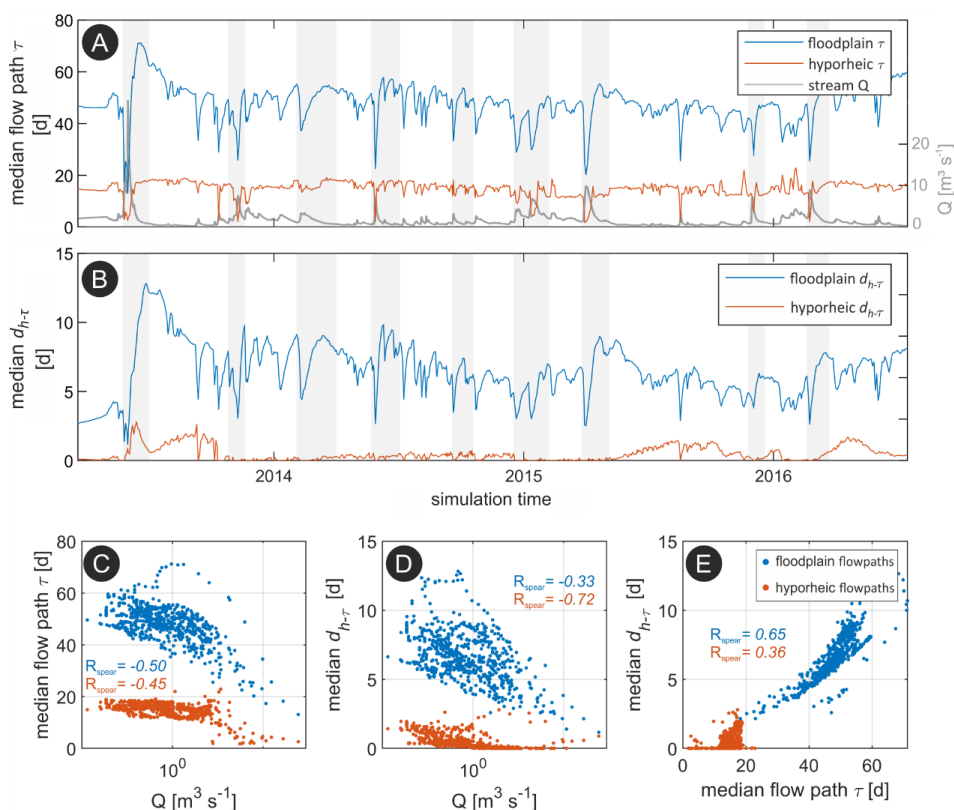
Fig.9: a) median transit-times (median flow path τ) alongside stream Q; **b)** median exposure-times (median $d_{h\text{-}\tau}$); **c)** median flow path *vs.* stream discharge (Q); **d)** median $d_{h\text{-}\tau}$ *vs.* Q; and **e)** median $d_{h\text{-}\tau}$ *vs.* median flow path τ. The Spearman's rank correlation (R_{spear}) between variables is showed in the scatter plots (c-e). Grey vertical bars (a-b) indicate discharge events periods. Note the log scale for Q values in (c-d).

The Fig.9b indicates that hyporheic $d_{h\text{-}\tau}$ increases under baseflow conditions relative to values during discharge events although hyporheic τ were somewhat constant over time (Fig.9a). Indeed, hyporheic $d_{h\text{-}\tau}$ were inversely correlated to stream discharge (R_{spear}= -0.72, Fig.9d), but only weakly correlated to variations of transit-times (R_{spear}= 0.36, Fig.9e). In contrast, for floodplain flow paths, $d_{h\text{-}\tau}$ was only slightly negative correlated with stream Q (R_{spear}= -0.33), whereas they showed a stronger correlation with flow path transit-times (R_{spear}= 0.65). Whereas both hyporheic and floodplain $d_{h\text{-}\tau}$ decrease with increasing Q due to overall shorter water transit-times, the occurrence and controls of mixing hot-spots due to flow dynamics at these different regions are somewhat different, as it will be discussed in Sect. 4.3.

4 Discussion

4.1 Validation of the flow model and the HMC results

In this study, we coupled a previously calibrated numerical flow model with the HMC method (Partington et al., 2011)
in order to assess the distribution of different water fractions in a stream corridor, using the riparian zone of the Selke
470   stream as a study case. The numerical model used here had been calibrated based on another observation period
(Nogueira et al., in press), but after implementation of correct hydrological BCs (e.g., stream inflow, groundwater
heads at the boundary) showed good agreement with field data from the period investigated in this paper. This
reinforces the quality of the original calibration and justifies the application of the numerical flow model to another
time period after BC adjustments. Small mismatches between observations and simulated values in terms of
475   groundwater heads and stream discharge could be related to the simplified geology within the numerical flow model,
which can affect SW-GW dynamics and groundwater flow paths (Fleckenstein et al., 2006; Gianni et al., 2019; Savoy
et al., 2017), as well as to the simplified streambed heterogeneity that can modify overall SW-GW exchange fluxes
(Pryshlak et al., 2015; Tang et al., 2017).

Usually, numerical flow models are solely calibrated based on hydrological observations. Previous studies using the
480   HMC method have rarely attempted to validate their results based on hydrochemical data, exceptions being the studies
by Liggett *et al.* (2015) and Berezowski *et al.* (2019), for instance, while this could further enhance model reliability
and parameterization (Partington et al., 2020; Schilling et al., 2017, 2019). Here, in addition to groundwater heads and
stream discharge evaluation, we verified the HMC results by comparing simulated f_{SW} and calculated F_{STR}, the latter
based on a Cl$^-$ mixing model. The calculation of F_{STR} was possible for most of the water samples (70%), whereas a
485   few of them presented unrealistic $F_{STR} > 1$ due to Cl$^-$ concentrations being temporally lower than in the stream water
end-member. We attribute this to local variability in evaporation or the presence of geogenic Cl$^-$ that can affect Cl$^-$
concentrations (Delsman et al., 2013; Ong et al., 1995). Nevertheless, the simulated f_{SW} values matched the field F_{STR}
values at the observation wells quite well, indicating a good performance of the HMC method for mapping water
source composition despite model simplifications. The small differences between F_{STR} and f_{SW} were acceptable given
490   that a calibration to hydrochemical data was not performed in this study, and that the model captured the main SW-
GW dynamics and hydrochemical variations, well which is further discussed in Sect. 4.5. These results suggest that
the HMC method can be a valuable tool, complementary to more labour-intensive field sampling, for mapping patterns
of water source composition and their temporal variation at the riparian zone and watershed scales (Berezowski et al.,
2019; Schilling et al., 2017).

495

4.2   HMC fractions and HZ dynamics

In terms of water origin there was a nearly constant distribution of the different HMC fractions within the model
domain (35% stream water, 35% groundwater, and 30% floodplain water). However, taking a look at the fully-
saturated domain only (70-80% of the total simulated domain), reveals that 90% of the water in the saturated zone
500   originates from the stream (50%) and from groundwater flowing into the domain via the upstream boundary (40%),
Fig.5a. This is manifested in a geochemical HZ (region presenting $f_{SW} \geq 0.5$) that extends up to 200 m into the riparian
aquifer. While this may appear as a large percentage of stream water in the riparian aquifer, other studies of alluvial

aquifers reported equally large percentages of stream water in the riparian aquifer at large distances from the stream (up to 250m), which were especially controlled by the permeability of the aquifer material (Schilling et al., 2017).

505 Similarly, Poole *et al.* (2008) have found that alluvial aquifer water at the Minthorn study site (gravel-alluvial dominated aquifer) was essentially all derived from the main stream channel of the Umatilla River. They also found that the *geochemical* HZ penetrates to the entire local riparian zone (about 300m wide) (Jones et al., 2008). In contrast, Sawyer *et al.* (2009) estimated the HZ extent to be only up to 30 m from the banks of the Colorado River near the Hornsby Bend site. In their case, however, the hydraulic conductivity of the aquifer material was nearly one order of

510 magnitude smaller than on the other sites and on ours (and the stream reach has not been predominantly losing). Those previous studies and our findings go in line with the propositions of Boulton *et al.* (1998) and Wondzell (2011) on the combined influence of hydrogeology and stream flow dynamics on the development of the hyporheic zone and exchanges around streams. Both studies have suggested that the cross-sectional area of the hyporheic zone relative to the stream channel are the highest for low-order streams, while unconstrained lowland streams present the greatest

515 hyporheic zone cross-sectional area relative to wetted stream channel (Boulton et al., 1998).

Within the local HZ, most of the water was advected stream water (approximately 80%). This is also in line with previous studies highlighting the dominance of purely advected surface water within hyporheic zones (Hester et al., 2014, 2019). Within the simulated domain, most of the infiltrated stream water did not immediately return to the stream and may therefore be termed "groundwater" after some transit through the aquifer. However, the fact that it

520 originated from the stream manifests in a different chemical composition compared to ambient groundwater. For instance, the infiltrated stream water will have higher contents of dissolved oxygen (DO) and dissolved organic carbon (DOC) compared to ambient groundwater (Trauth et al., 2018). In turn, the mixing between the infiltrated SW and ambient GW, can deliver DOC as an electron donor to facilitate denitrification of groundwater-borne nitrate (Hester et al., 2019; Song et al., 2018; Trauth et al., 2014; Trauth and Fleckenstein, 2017).

525 **4.3 Variations and controls of mixing degrees and mixing hot-spots**

Only a few studies attempted to quantify the spatio-temporal variations of the mixing degrees resulting from SW-GW exchange process at the stream-corridor scale (Lessels et al., 2016), as well as their potential implications for biogeochemical processes. While some studies have relied on extensive field campaigns (Gassen et al., 2017; Jones et al., 2014), numerical simulations carried out by Trauth & Fleckenstein (2017) and Hester et al. (2019), suggested

530 the importance of mixing zones for the denitrification of groundwater-borne nitrate. Here, on average, nearly 50% of the model domain presented $d \geq 0.25$ throughout the simulation period. About 9% of the domain (and roughly 20% of the HZ) could be defined as *mixing hot-spots* ($d \geq 0.75$), with most of them being located at the fringe of the HZ. The persistence of these mixing hot-spots in time could be illustrated with the metric max_d/σ_d, which was consistently high at the fringe of the HZ. This is qualitatively consistent with previous smaller-scale studies showing that mixing

535 hot-spots between SW-GW tend to occur in narrow zones at the fringe of the HZ (Hester et al., 2013; Sawyer and Cardenas, 2009; Trauth and Fleckenstein, 2017). Likewise, Berezowski *et al.* (2019) computed d_h values slightly

above 6% of the total area of a larger basin in Poland following a large flood event, d_h that were also mainly located at the fringe of the HZ.

In our simulations, magnitudes of peak discharges during events were strongly correlated with increases of d_h over the event. This is in line with Trauth & Fleckenstein (2017), who found that for the same event duration, discharge events with higher peaks increased denitrification of groundwater-borne nitrate by a factor of up to 7x due to enhanced mixing with stream-borne DOC. In the same way, Hester et al. (2019) showed that the size of the SW-GW mixing zone below a streambed dune increased and shifted with increasing SW depth (analogous to increasing stream discharge in this study). While our results indicated a similar expansion of the mixing zones following discharge events (Fig.8c), we could also observe and quantify the temporal shift of d_h peaks (e.g., counter-clockwise hysteresis with a peak of stream discharge events) alongside the shift of their locations within the riparian zone.

Water transit-times are usually used as a metric to assess the HZ reactive potential since the longer the transit-time, the higher the potential for solute transformations (Boano et al., 2010; Zarnetske et al., 2011). To evaluate this potential in relation to reactive mixing zones we defined the exposure-time ($d_{h\text{-}\tau}$), as the time water resides within model cells classified as mixing hot-spots. Our results show that the hyporheic $d_{h\text{-}\tau}$ were generally smaller than (non-hyporheic) floodplain $d_{h\text{-}\tau}$ and more negatively correlated with stream discharge (Fig.9d). This is mainly because hyporheic transit-times are generally shorter than floodplain water transit-times. Besides, under low stream discharge conditions, ambient groundwater flow is somewhat more parallel to the stream (Nogueira et al., in press), while groundwater flow towards the stream increases due to a decrease in SW depth (Buffington and Tonina, 2009). This and the slightly stronger gaining conditions at the pool located further downstream in the model domain (Fig.S3, supplementary material) result in a greater SW-GW mixing near the stream region, hence increasing the hyporheic $d_{h\text{-}\tau}$. With increasing stream discharge, however, SW influx into the riparian aquifer increases, which shifts the SW-GW mixing front to regions farther from the stream (Hester et al., 2019) and hyporheic $d_{h\text{-}\tau}$ decreases.

In contrast, with distance from the stream, $d_{h\text{-}\tau}$ is mainly controlled by variations in water transit-times. This is because mixing far from the stream is mainly enhanced by increasing stream discharge, which brings SW to farther distances within the aquifer where it can mix with ambient groundwater. In line with our results, Trauth et al. (2015) found the total consumption of groundwater-borne nitrate within an instream gravel bar to be higher under neutral and slightly gaining ambient groundwater conditions (i.e., low stream discharge). This is when the total influx of solutes from the stream is low, but consumption of groundwater-borne nitrate is high due to enhanced SW-GW mixing. Likewise, our results suggest that discharge events can enhance turnover of groundwater-borne solutes in the riparian zone at locations farther from the stream more than in the hyporheic regions near the stream. Conversely, under low discharge conditions, hyporheic $d_{h\text{-}\tau}$ increase due to slightly increasing GW upwelling and subsequent SW-GW mixing. Nevertheless, in strongly gaining stream reaches with a dominance of GW-seepage to the stream (e.g., limited or absent hyporheic flow paths), hyporheic transit-times (Cardenas, 2009; Trauth et al., 2013, 2014), as well as SW-GW mixing (e.g., in terms of flux magnitude) (Hester et al., 2013; Sawyer et al., 2009) would be smaller, and consequently the potential for turnover of groundwater-borne solutes would be smaller too (Hester et al., 2019).

4.4 Mixing hot-spots and biogeochemical implications

In order to further show the implications of mixing for local biogeochemical processes, we compared our HMC results with hydrochemical analyses from Gassen et al. (2017), who monitored water quality across the groundwater-table interface using a local multilevel piezometer that can be sampled at highly resolved depth intervals in the variably saturated vadose and fully saturated groundwater zones (Fig.S6, supplementary material).
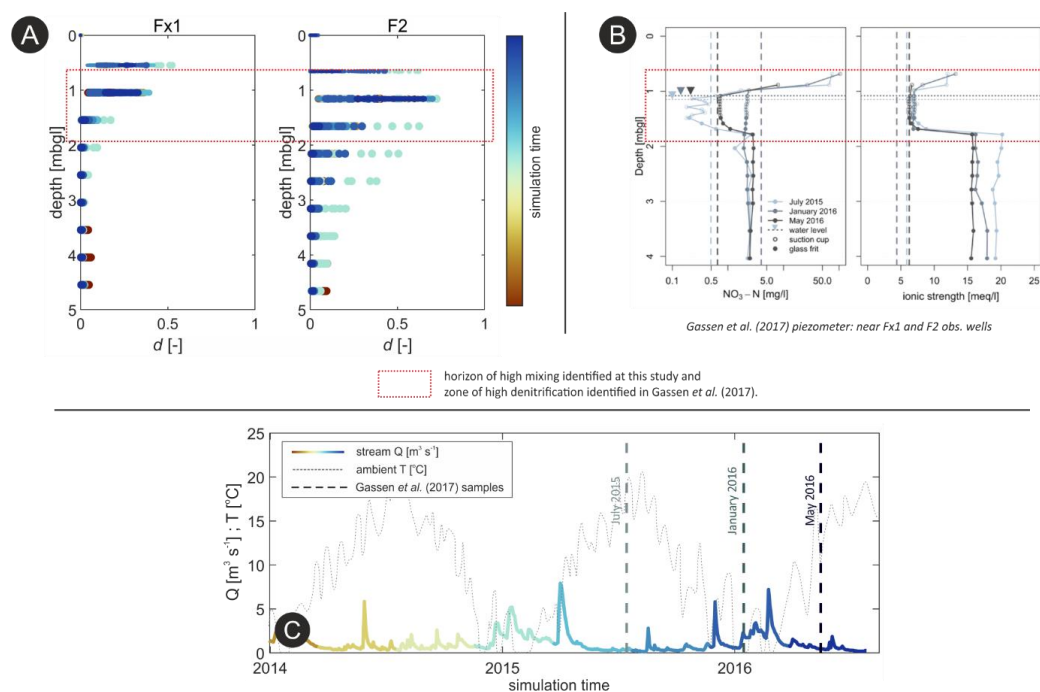
Fig.10: a) mixing degrees with depth for two observation wells. Colours indicate simulation time; **b)** measurements of NO3−N concentrations and ionic strength in a multilevel piezometer for three different sampling dates. Vertical dashed lines represent NO3−N concentrations/ionic strength of the stream water, horizontal dotted lines represent the groundwater-table at the corresponding sampling date (reprinted (adapted) with permission from Gassen et al. (2017), Copyright (2017), American Chemical Society); and **c)** ambient temperature alongside stream Q coloured according to simulation time. Vertical dashed lines indicate the sampling dates from Gassen et al. (2017).

The HMC-simulated vertical variations of mixing degrees at the near stream observation wells show strong similarity with observed vertical variations in nitrate concentrations and a denitrification fringe around the water table separating high concentrations in the vadose zone form significantly lower concentrations in the saturated zone as highlighted by the red rectangle in Fig.10a and Fig.10b. Our simulations revealed generally higher mixing degrees ($d \geq 0.5$) over the top 1-2m of the saturated zone, while Gassen et al. (2017) observed high nitrate concentrations above the groundwater table (up to 70 mg L^{-1}),which exponentially decreased across the uppermost saturated zone to values below 3 mg L^{-1}.

Besides seasonal temperature effects on denitrification rates (Fig.10c) (Nogueira et al., 2021; Widdowson et al., 1988; Zheng et al., 2016), mixing with stream-borne DOC and subsequent denitrification is most likely the processes responsible for the observed high denitrification rates at the vadose zone-groundwater interface in the uppermost parts of the saturated zone. This reinforces the importance of mixing hot-spots for biogeochemical processes in riparian zones and highlights the importance of mapping different water sources and their mixing dynamics.

4.5 Limitations of the employed method and recommendations for future studies

Despite good agreement with field F_{STR} values, simulated HMC water fractions such as f_{SW} were not included in the calibration of the numerical model. In a more rigorous calibration, this could have been done, which might further minimize mismatches between simulated and observed HMC fractions, while still respecting the parameter range. It is a trade-off with computation time since model calibration can largely increase with sub-routines for the calculation of observations/parameters of interest. Since the numerical model used here was previously calibrated based on both conventional and more unconventional oservations, and since the goal of this study was not to reproduce all details at the field site, we did not carry out additional model calibration. However, the addition of unconventional observation-types to model calibration (on the top of commonly used groundwater heads and stream stage/discharge measurements) tends to lead to a more robust calibration reducing equifinality in the parameter sets (Nogueira *et al.,* in press; Schilling *et al.*, 2017, 2019; Partington *et al.*, 2020), and should be considered in future studies.

We intentionally did not conduct explicit simulations of reactive transport in this study to save on computational costs. Such simulations would have allowed a comparison of observed and simulated concentration values and their dynamics for a more rigorous evaluation of model performance (Nogueira et al., in press). However, our model results could match patterns of mixing degrees estimated from field observations very well and the simulated patterns allowed an improved interpretation of observed concentrations. Furthermore our results were well in line with other studies on biogeochemical processes related to SW-GW mixing at comparable sites. The identification of hot-spots for macroscopic mixing between SW-GW with the HMC method can provide a good proxy for the occurrence of potential biogeochemical hot-spots for mixing-dependent turnover of groundwater-borne solutes in river corridors. However, care should be taken in interpreting such results as this "potential" may not be realized if stream-borne reactants (like DOC) have been exhausted before reaching the mixing hot-spots.

Finally, the HMC method is based on water fluxes computed between model cells and therefore assumes that all HMC fractions are perfectly mixed within a model cell at every time-step (Partington et al., 2011). This condition may be violated, if stratification of different waters exist over the vertical extent of a model cell (Karan et al., 2013; Kolbe et al., 2019). Although the vertical extent of the model cells in our study is much smaller than the extent over which significant stratification would commonly be assumed to occur, high-resolution local observations (e.g., of vertical concentration variations) may not be captured with our approach, which integrates over the scale of larger model cells.

5 Conclusion

Riparian zones contain waters from different sources, which can mix with each other and in turn enable mixing-dependent biogeochemical processing. In this study, we coupled a hydraulic mixing cell (HMC) method with a previously-calibrated transient and fully-integrated 3D numerical flow model to assess the distribution of different water sources in a riparian aquifer, as well as their mixing dynamics. The simulated mixing degrees matched estimated values based on natural chloride tracer data well. A qualitative comparison of HMC based mixing patterns with concentration patterns from additional, hydrochemical data generally confirmed the robustness of the method, which is computationally comparably cheap, as it does not require explicit solute transport simulations to track different water sources in space and time.

Our estimations indicated that along the simulated stream reach, about 50% of the water in the riparian aquifer originates from the stream, whereas about 40% is groundwater and the remaining 10% is floodplain water (e.g., from rainfall or flooding from top soil). This overall composition was relatively steady over time, but it was episodically affected by larger stream discharge events, which deliver larger volumes of stream water to the riparian aquifer via infiltration or overbank flow. Similarly, macroscopic mixing, evaluated in terms of the mixing-degrees, was observed at least in 80% of the domain ($d > 0$), but it was spatially and temporally variable within the riparian zone. On average, about 9% of the aquifer volume could be characterized as mixing hot-spots ($d \geq 0.75$), but this percentage could be nearly 1.5 times higher following large discharge events. Moreover, event intensity (event peak magnitude) was found to be more important for the increase of the spatial extent of mixing hot-spots than event duration. Our modelling results also indicate that event-driven changes in the fluxes and velocity of infiltrating stream water, affect exposure-times (i.e., time of a water parcel residing within a *mixing hot-spot*) along hyporheic flow paths to a larger extent than the exposure-times of water flowing far from the stream. With distance from the stream, exposure-times become increasingly controlled by variations in general water transit-times. In contrast, in the near stream zone, the rapid increase of SW influx during events shifts the ratio between the water fractions to SW, reducing the extent of potential mixing zones inhibiting mixing dependent reactions. At the same time increasing stream water infiltration at higher flow velocities delivers stream water further into the riparian aquifer, shifting the zones with significant macroscopic mixing between SW and GW away from the near stream zone.

The analysis of water source dynamics, and of the relationship between the mixing of different water sources and flow dynamics in a riparian zone presented in this study provides an easy-to-transfer approach for the mapping of water sources and the identification of *mixing hot-spots* within riparian zones. Understanding the patterns and dynamics of macroscopic mixing between SW and GW in riparian zones can help to better understand patterns of reactive turnover or the redistribution of other, non-reactive solutes or small particulate substances (e.g., micro plastic particles) in the riparian zone. Future assessments could also focus on smaller scale streambed mixing processes, considering, for instance, (1) more heterogeneous hydraulic conductivity fields at the streambed and at the riparian aquifer, as well as (2) different events duration and peak magnitudes.

6   Data availability

665   The field data, and the numerical model files are publically available and can be assessed through:
http://www.hydroshare.org/resource/a0dc51142fe249f89877c4005e0b6947.

7   Author contributions

GN performed the formal analysis, the investigation and wrote the original draft of the manuscript; all the authors
670   contributed to review, final writing and editing; GN, CS, and JF conceptualized the study; GN, DP, PB, and JF
conceived the methodology; GN, CS, DP, and JF worked on the validation of the study; CS and JF were responsible
for supervision; JF was responsible for funding acquisition, resources and project administration.

8   Acknowledgment

675   This research was financially supported by the ENIGMA-ITN project within the European Union's Horizon 2020
research and innovation programme under the Marie Sklodowska-Curie Grant Agreement No.722028, as well as the
Collaborative Research Centre 1357 MICROPLASTICS funded by the German Research Foundation (DFG) Project
Number 391977956 – SFB 1357 and the Research Program of the Helmholtz Association.

9   References

680   Appelo, C. A. J. and Postma, D.: Geochemistry, Groundwater and Pollution - 2nd Edition, A.A. BALKEMA
PUBLISHERS, Amsterdam., 2005.

Aquanty Inc.: HydroGeoSphere Reference Manual, Waterloo. [online] Available from:
https://www.aquanty.com/hgs-download, 2015.

685   Battin, T. J.: Hydrologic flow paths control dissolved organic carbon fluxes and metabolism in an alpine stream
hyporheic zone, , 35(10), 3159–3169, 1999.

Bear, J. and Verruijt, A.: Modeling Groundwater Flow and Pollution, 1st ed., edited by J. Bear, D. Reidel Publishing
Company, Dordrecht., 1987.

Berezowski, T., Partington, D., Chormański, J. and Batelaan, O.: Spatiotemporal Dynamics of the Active Perirheic
690   Zone in a Natural Wetland Floodplain, Water Resour. Res., 55(11), 9544–9562, doi:10.1029/2019WR024777, 2019.

Bernhardt, E. S., Blaszczak, J. R., Ficken, C. D., Fork, M. L., Kaiser, K. E. and Seybold, E. C.: Control Points in
Ecosystems: Moving Beyond the Hot Spot Hot Moment Concept, Ecosystems, 20(4), 665–682, doi:10.1007/s10021-
016-0103-y, 2017.

Biehler, A., Chaillou, G., Buffin-Bélanger, T. and Baudron, P.: Hydrological connectivity in the aquifer–river
695   continuum: Impact of river stages on the geochemistry of groundwater floodplains, J. Hydrol., 590, 125379,
doi:10.1016/j.jhydrol.2020.125379, 2020.

Boano, F., Demaria, A., Revelli, R. and Ridolfi, L.: Biogeochemical zonation due to intrameander hyporheic flow, Water Resour. Res., 46(2), 1–13, doi:10.1029/2008WR007583, 2010.

Boulton, A. J., Findlay, S., Marmonier, P., Stanley, E. H. and Valett, H. M.: The Functional Significance of the Hyporheic Zone in Streams and Rivers, Annu. Rev. Ecol. Syst., 29(1), 59–81, doi:10.1146/annurev.ecolsys.29.1.59, 1998.

Broecker, T., Sobhi Gollo, V., Fox, A., Lewandowski, J., Nützmann, G., Arnon, S. and Hinkelmann, R.: High-Resolution Integrated Transport Model for Studying Surface Water–Groundwater Interaction, Groundwater, 1–15, doi:10.1111/gwat.13071, 2021.

Buffington, J. M. and Tonina, D.: Hyporheic exchange in mountain rivers II: Effects of channel morphology on mechanics, scales, and rates of exchange, Geogr. Compass, 3(3), 1038–1062, doi:10.1111/j.1749-8198.2009.00225.x, 2009.

Cardenas, M. B.: Stream-aquifer interactions and hyporheic exchange in gaining and losing sinuous streams, Water Resour. Res., 45(6), 1–13, doi:10.1029/2008WR007651, 2009.

Cirpka, O. A. and Kitanidis, P. K.: Characterization of mixing and dilution in heterogeneous aquifers by means of local temporal moments, Water Resour. Res., 36(5), 1221–1236, doi:10.1029/1999WR900354, 2000.

Delsman, J. R., Essink, G. H. P. O., Beven, K. J. and Stuyfzand, P. J.: Uncertainty estimation of end-member mixing using generalized likelihood uncertainty estimation (GLUE), applied in a lowland catchment, Water Resour. Res., 49(8), 4792–4806, doi:10.1002/wrcr.20341, 2013.

Dentz, M., Le Borgne, T., Englert, A. and Bijeljic, B.: Mixing, spreading and reaction in heterogeneous media: A brief review, J. Contam. Hydrol., 120–121(C), 1–17, doi:10.1016/j.jconhyd.2010.05.002, 2011.

Doherty, J.: PEST: Model-independent parameter estimation. User Manual, , 368, 2018.

Fleckenstein, J. H., Niswonger, R. G. and Fogg, G. E.: River-aquifer interactions, geologic heterogeneity, and low-flow management, Ground Water, 44(6), 837–852, doi:10.1111/j.1745-6584.2006.00190.x, 2006.

Gassen, N., Griebler, C., Werban, U., Trauth, N. and Stumpp, C.: High Resolution Monitoring Above and Below the Groundwater Table Uncovers Small-Scale Hydrochemical Gradients, Environ. Sci. Technol., 51, 9, doi:10.1021/acs.est.7b03087, 2017.

Gianni, G., Doherty, J. and Brunner, P.: Conceptualization and Calibration of Anisotropic Alluvial Systems: Pitfalls and Biases, Groundwater, 57(3), 409–419, doi:10.1111/gwat.12802, 2019.

Gomez-Velez, J. D., Wilson, J. L., Cardenas, M. B. and Harvey, J. W.: Flow and Residence Times of Dynamic River Bank Storage and Sinuosity-Driven Hyporheic Exchange, Water Resour. Res., 53(10), 8572–8595, doi:10.1002/2017WR021362, 2017.

Gooseff, M. N.: Defining hyporheic zones - advancing our conceptual and operational definitions of where stream water and groundwater meet, Geogr. Compass, 4(8), 945–955, doi:10.1111/j.1749-8198.2010.00364.x, 2010.

Gu, C., Anderson, W. and Maggi, F.: Riparian biogeochemical hot moments induced by stream fluctuations, Water Resour. Res., 48(9), 1–17, doi:10.1029/2011WR011720, 2012.

Gupta, H. V., Kling, H., Yilmaz, K. K. and Martinez, G. F.: Decomposition of the mean squared error and NSE performance criteria: Implications for improving hydrological modelling, J. Hydrol., 377(1–2), 80–91, doi:10.1016/j.jhydrol.2009.08.003, 2009.

Gutiérrez-Jurado, K. Y., Partington, D., Batelaan, O., Cook, P. and Shanafield, M.: What Triggers Streamflow for Intermittent Rivers and Ephemeral Streams in Low-Gradient Catchments in Mediterranean Climates, Water Resour. Res., 55(11), 9926–9946, doi:10.1029/2019WR025041, 2019.

Hester, E. T., Young, K. I. and Widdowson, M. A.: Mixing of surface and groundwater induced by riverbed dunes: Implications for hyporheic zone definitions and pollutant reactions, Water Resour. Res., 49(9), 5221–5237, doi:10.1002/wrcr.20399, 2013.

Hester, E. T., Young, K. I. and Widdowson, M. A.: Controls on mixing-dependent denitrification in hyporheic zones induced by riverbed dunes: A steady state modeling study, Water Resour. Res., 50(11), 9048–9066, doi:10.1002/2014WR015424, 2014.

745   Hester, E. T., Cardenas, M. B., Haggerty, R. and Apte, S. V.: The importance and challenge of hyporheic mixing, Water Resour. Res., 53(5), 3565–3575, doi:10.1002/2016WR020005, 2017.

Hester, E. T., Eastes, L. A. and Widdowson, M. A.: Effect of Surface Water Stage Fluctuation on Mixing-Dependent Hyporheic Denitrification in Riverbed Dunes, Water Resour. Res., 55(6), 4668–4687, doi:10.1029/2018WR024198, 2019.

Hill, A. R.: Nitrate Removal in Stream Riparian Zones, J. Environ. Qual., 25(4), 743–755, 750   doi:10.2134/jeq1996.00472425002500040014x, 1996.

Jencso, K. G., McGlynn, B. L., Gooseff, M. N., Bencala, K. E. and Wondzell, S. M.: Hillslope hydrologic connectivity controls riparian groundwater turnover: Implications of catchment structure for riparian buffering and stream water sources, Water Resour. Res., 46(10), 1–18, doi:10.1029/2009WR008818, 2010.

Jones, C. N., Scott, D. T., Edwards, B. L. and Keim, R. F.: Perirheic mixing and biogeochemical processing in flow-755   through and backwater floodplain wetlands, Water Resour. Res., 50(9), 7394–7405, doi:10.1002/2014WR015647, 2014.

Jones, K. L., Poole, G. C., Woessner, W. W., Vitale, M. V., Boer, B. R., O'Daniel, S. J., Thomas, S. A. and Geffen, B. A.: Geomorphology, hydrology, and aquatic vegetation drive seasonal hyporheic flow patterns across a gravel-dominated floodplain, Hydrol. Process., 22(13), 2105–2113, doi:10.1002/hyp.6810, 2008.

760   Karan, S., Engesgaard, P., Looms, M. C., Laier, T. and Kazmierczak, J.: Groundwater flow and mixing in a wetland-stream system: Field study and numerical modeling, J. Hydrol., 488, 73–83, doi:10.1016/j.jhydrol.2013.02.030, 2013.

Kitanidis, K.: The concept of the dilution index, , 30(7), 2011–2026, doi:https://doi.org/10.1029/94WR00762, 1994.

Knoben, W. J. M., Freer, J. E. and Woods, R. A.: Technical note: Inherent benchmark or not? Comparing Nash-765   Sutcliffe and Kling-Gupta efficiency scores, Hydrol. Earth Syst. Sci. Discuss., (July), 1–7, doi:10.5194/hess-2019-327, 2019.

Kolbe, T., de Dreuzy, J.-R., Abbott, B. W., Aquilina, L., Babey, T., Green, C. T., Fleckenstein, J. H., Labasque, T., Laverman, A. M., Marçais, J., Peiffer, S., Thomas, Z. and Pinay, G.: Stratification of reactivity determines nitrate removal in groundwater, Proc. Natl. Acad. Sci., 116(7), 2494–2499, doi:10.1073/pnas.1816892116, 2019.

770   Kollet, S. J. and Maxwell, R. M.: Integrated surface-groundwater flow modeling: A free-surface overland flow boundary condition in a parallel groundwater flow model, Adv. Water Resour., 29(7), 945–958, doi:10.1016/j.advwatres.2005.08.006, 2006.

Lawrence, J. E., Skold, M. E., Hussain, F. A., Silverman, D. R., Resh, V. H., Sedlak, D. L., Luthy, R. G. and McCray, J. E.: Hyporheic zone in urban streams: A review and opportunities for enhancing water quality and 775   improving aquatic habitat by active management, Environ. Eng. Sci., 30(8), 480–501, doi:10.1089/ees.2012.0235, 2013.

Lessels, J. S., Tetzlaff, D., Birkel, C., Dick, J. and Soulsby, C.: Water sources and mixing in riparian wetlands revealed by tracers and geospatial analysis, Water Resour. Res., 52(1), 456–470, doi:10.1002/2015WR017519, 2016.

780   Liggett, J. E., Partington, D., Frei, S., Werner, A. D., Simmons, C. T. and Fleckenstein, J. H.: An exploration of coupled surface-subsurface solute transport in a fully integrated catchment model, J. Hydrol., 529, 969–979, doi:10.1016/j.jhydrol.2015.09.006, 2015.

Liu, S. and Chui, T. F. M.: Impacts of different rainfall patterns on hyporheic zone under transient conditions, J. Hydrol., 561(April), 598–608, doi:10.1016/j.jhydrol.2018.04.019, 2018.

785   Mayer, P. M., Reynolds, S. K. and Canfield, T. J.: Riparian buffer width, vegetative cover, and nitrogen removal

effectiveness: a review of current science and regulations., Epa/600/R-05/118, 1–40 [online] Available from: http://nepis.epa.gov/Exe/ZyPDF.cgi/2000O182.PDF?Dockey=2000O182.PDF, 2006.

McCallum, J. L., Cook, P. G., Brunner, P. and Berhane, D.: Solute dynamics during bank storage flows and implications for chemical base flow separation, Water Resour. Res., 46(7), 1–11, doi:10.1029/2009WR008539, 2010.

McClain, M. E., Boyer, E. W., Dent, C. L., Gergel, S. E., Grimm, N. B., Groffman, P. M., Hart, S. C., Harvey, J. W., Johnston, C. A., Mayorga, E., McDowell, W. H. and Pinay, G.: Biogeochemical Hot Spots and Hot Moments at the Interface of Terrestrial and Aquatic Ecosystems, Ecosystems, 6(4), 301–312, doi:10.1007/s10021-003-0161-9, 2003.

Mertes, L. A. K.: Documentation and significance of the perirheic zone on inundated floodplains, Water Resour. Res., 33(7), 1749–1762, doi:10.1029/97WR00658, 1997.

Mirus, B. B., Ebel, B. A., Heppner, C. S. and Loague, K.: Assessing the detail needed to capture rainfall-runoff dynamics with physics-based hydrologic response simulation, Water Resour. Res., 47(6), 1–18, doi:10.1029/2010WR009906, 2011.

Nogueira, G. E. H., Schmidt, C., Trauth, N. and Fleckenstein, J. H.: Seasonal and short-term controls of riparian oxygen dynamics and the implications for redox processes, Hydrol. Process., 35(2), 16, doi:10.1002/hyp.14055, 2021.

Nogueira, G. E. H., Schmidt, C., Brunner, P., Graeber, D. and Fleckenstein, J. H.: Transit-time and temperature control the spatial patterns of aerobic respiration and denitrification in the riparian zone, Water Resources Research, *in press*.

Nogueira, G. E. H., C. Schmidt, D. Partington, P. Brunner, J. h. Fleckenstein: Spatio-temporal variations of water sources and mixing spots in a riparian zone: supplementary data, HydroShare, http://www.hydroshare.org/resource/a0dc51142fe249f89877c4005e0b6947, 2021.

Ocampo, C. J., Oldham, C. E. and Sivapalan, M.: Nitrate attenuation in agricultural catchments: Shifting balances between transport and reaction, Water Resour. Res., 42(1), 1–16, doi:10.1029/2004WR003773, 2006.

Ong, C. G., Tanji, K. K., Dahlgren, R. A., Smith, G. R. and Quek, A. F.: Water Quality and Trace Element Evapoconcentration in Evaporation Ponds for Agricultural Waste Water Disposal, J. Agric. Food Chem., 43(7), 1941–1947, doi:10.1021/jf00055a034, 1995.

Partington, D., Brunner, P., Simmons, C. T., Therrien, R., Werner, A. D., Dandy, G. C. and Maier, H. R.: A hydraulic mixing-cell method to quantify the groundwater component of streamflow within spatially distributed fully integrated surface water-groundwater flow models, Environ. Model. Softw., 26(7), 886–898, doi:10.1016/j.envsoft.2011.02.007, 2011.

Partington, D., Brunner, P., Simmons, C. T., Werner, A. D., Therrien, R., Maier, H. R. and Dandy, G. C.: Evaluation of outputs from automated baseflow separation methods against simulated baseflow from a physically based, surface water-groundwater flow model, J. Hydrol., 458–459, 28–39, doi:10.1016/j.jhydrol.2012.06.029, 2012.

Partington, D., Brunner, P., Frei, S., Simmons, C. T., Werner, A. D., Therrien, R., Maier, H. R., Dandy, G. C. and Fleckenstein, J. H.: Interpreting streamflow generation mechanisms from integrated surface-subsurface flow models of a riparian wetland and catchment, Water Resour. Res., 49(9), 5501–5519, doi:10.1002/wrcr.20405, 2013.

Partington, D., Knowling, M. J., Simmons, C. T., Cook, P. G., Xie, Y., Iwanaga, T. and Bouchez, C.: Worth of hydraulic and water chemistry observation data in terms of the reliability of surface water-groundwater exchange flux predictions under varied flow conditions, J. Hydrol., 590(November 2019), 125441, doi:10.1016/j.jhydrol.2020.125441, 2020.

Pinay, G., Ruffinoni, C., Wondzell, S. and Gazelle, F.: Change in groundwater nitrate concentration in a large river floodplain: Denitrification, uptake, or mixing?, J. North Am. Benthol. Soc., 17(2), 179–189, doi:10.2307/1467961, 1998.

Pinay, G., Peiffer, S., Dreuzy, J. De, Krause, S., Hannah, D. M., Fleckenstein, J. H., Sebilo, M., Bishop, K. and

Hubert-moy, L.: Upscaling Nitrogen Removal Capacity from Local Hotspots to Low Stream Orders ' Drainage Basins, Ecosystems, 18(6), 1101–1120, doi:10.1007/s10021-015-9878-5, 2015.

Poole, G. C., O'Daniel, S. J., Jones, K. L., Woessner, W. W., Bernhardt, E. S., Helton, A. M., Stanford, J. A., Boer, B. R. and Beechie, T. J.: Hydrologic spiralling: the role of multiple interactive flow paths in stream ecosystems,
835   River Res. Appl., 24(7), 1018–1031, doi:10.1002/rra.1099, 2008.

Pryshlak, T. T., Sawyer, A. H., Stonedahl, S. H. and Soltanian, M. R.: Multiscale hyporheic exchange through strongly heterogeneous sediments, Water Resour. Res., 51(11), 9127–9140, doi:10.1002/2015WR017293, 2015.

Ranalli, A. J. and Macalady, D. L.: The importance of the riparian zone and in-stream processes in nitrate attenuation in undisturbed and agricultural watersheds - A review of the scientific literature, J. Hydrol., 389(3–4),
840   406–415, doi:10.1016/j.jhydrol.2010.05.045, 2010.

Savoy, H., Kalbacher, T., Dietrich, P. and Rubin, Y.: Geological heterogeneity: Goal-oriented simplification of structure and characterization needs, Adv. Water Resour., 109, 1–13, doi:10.1016/j.advwatres.2017.08.017, 2017.

Sawyer, A. H.: Enhanced removal of groundwater-borne nitrate in heterogeneous aquatic sediments, Geophys. Res. Lett., 42(2), 403–410, doi:10.1002/2014GL062234, 2015.

845   Sawyer, A. H. and Cardenas, M. B.: Hyporheic flow and residence time distributions in heterogeneous cross-bedded sediment, Water Resour. Res., 45(8), 1–12, doi:10.1029/2008WR007632, 2009.

Sawyer, A. H., Cardenas, M. B., Bomar, A. and Mackey, M.: Impact of dam operations on hyporheic exchange in the riparian zone of a regulated river, Hydrol. Process., 23(15), 2129–2137, doi:10.1002/hyp.7324, 2009.

Sawyer, A. H., Kaplan, L. A., Lazareva, O. and Michael, H. A.: Hydrologic dynamics and geochemical responses
850   within a floodplain aquifer and hyporheic zone during Hurricane Sandy, Water Resour. Res., 50(6), 4877–4892, doi:10.1002/2013WR015101, 2014.

Schilling, O. S., Gerber, C., Partington, D. J., Purtschert, R., Brennwald, M. S., Kipfer, R., Hunkeler, D. and Brunner, P.: Advancing Physically-Based Flow Simulations of Alluvial Systems Through Atmospheric Noble Gases and the Novel37Ar Tracer Method, Water Resour. Res., 53(12), 10465–10490, doi:10.1002/2017WR020754, 2017.

855   Schilling, O. S., Cook, P. G. and Brunner, P.: Beyond Classical Observations in Hydrogeology: The Advantages of Including Exchange Flux, Temperature, Tracer Concentration, Residence Time, and Soil Moisture Observations in Groundwater Model Calibration, Rev. Geophys., 57(1), 146–182, doi:10.1029/2018RG000619, 2019.

Schmadel, N. M., Ward, A. S., Kurz, M. J., Fleckenstein, J. H., Zarnetske, J. P., Hannah, D. M., Blume, T., Vieweg, M., Blaen, P. J., Schmidt, C., Knapp, J. L. A., Klaar, M. J., Romeijn, P., Datry, T., Keller, T., Folegot, S., Arricibita,
860   A. I. M. and Krause, S.: Stream solute tracer timescales changing with discharge and reach length confound process interpretation, Water Resour. Res., 52(4), 3227–3245, doi:10.1002/2015WR018062, 2016.

Schneider, P., Vogt, T., Schirmer, M., Doetsch, J., Linde, N., Pasquale, N., Perona, P. and Cirpka, O. A.: Towards improved instrumentation for assessing river-groundwater interactions in a restored river corridor, Hydrol. Earth Syst. Sci., 15(8), 2531–2549, doi:10.5194/hess-15-2531-2011, 2011.

865   Song, X., Chen, X., Stegen, J., Hammond, G., Song, H., Dai, H., Graham, E. and Zachara, J. M.: Drought Conditions Maximize the Impact of High-Frequency Flow Variations on Thermal Regimes and Biogeochemical Function in the Hyporheic Zone, Water Resour. Res., 54(10), 7361–7382, doi:10.1029/2018WR022586, 2018.

Stegen, J. C., Fredrickson, J. K., Wilkins, M. J., Konopka, A. E., Nelson, W. C., Arntzen, E. V., Chrisler, W. B., Chu, R. K., Danczak, R. E., Fansler, S. J., Kennedy, D. W., Resch, C. T. and Tfaily, M.: Groundwater-surface water
870   mixing shifts ecological assembly processes and stimulates organic carbon turnover, Nat. Commun., 7, doi:10.1038/ncomms11237, 2016.

Stigter, T. Y., Van Ooijen, S. P. J., Post, V. E. A., Appelo, C. A. J. and Carvalho Dill, A. M. M.: A hydrogeological and hydrochemical explanation of the groundwater composition under irrigated land in a Mediterranean environment, Algarve, Portugal, J. Hydrol., 208(3–4), 262–279, doi:10.1016/S0022-1694(98)00168-1, 1998.

875   Tang, Q., Kurtz, W., Schilling, O. S., Brunner, P., Vereecken, H. and Hendricks Franssen, H. J.: The influence of

riverbed heterogeneity patterns on river-aquifer exchange fluxes under different connection regimes, J. Hydrol., 554, 383–396, doi:10.1016/j.jhydrol.2017.09.031, 2017.

Therrien, R., McLaren, R. G., Sudicky, E. A. and Panday, S. M.: HydroGeoSphere. A three-dimensional numerical model describing fully-integrated subsurface and surface flow and solute transport, Groundw. Simulations Gr., 457, doi:10.5123/S1679-49742014000300002, 2010.

Trauth, N. and Fleckenstein, J. H.: Single discharge events increase reactive efficiency of the hyporheic zone, Water Resour. Res., 53(Jan), 779–798, doi:10.1111/j.1752-1688.1969.tb04897.x, 2017.

Trauth, N., Schmidt, C., Maier, U., Vieweg, M. and Fleckenstein, J. H.: Coupled 3-D stream flow and hyporheic flow model under varying stream and ambient groundwater flow conditions in a pool-riffle system, Water Resour. Res., 49(9), 5834–5850, doi:10.1002/wrcr.20442, 2013.

Trauth, N., Schmidt, C., Vieweg, M., Maier, U. and Fleckenstein, J. H.: Hyporheic transport and biogeochemical reactions in pool-riffle systems under varying ambient groundwater flow conditions, J. Geophys. Res. Biogeosciences, 119(5), 910–928, doi:10.1002/2013JG002586, 2014.

Trauth, N., Schmidt, C., Vieweg, M., Oswald, S. E. and Fleckenstein, J. H.: Hydraulic controls of in-stream gravel bar hyporheic exchange and reactions, Water Resour. Res., 51(4), 2243–2263, doi:10.1002/2014WR015857, 2015.

Trauth, N., Musolff, A., Knöller, K., Kaden, U. S., Keller, T., Werban, U. and Fleckenstein, J. H.: River water infiltration enhances denitrification efficiency in riparian groundwater, Water Res., 130, 185–199, doi:10.1016/j.watres.2017.11.058, 2018.

Triska, F. J., Kennedy, V. C., Avanzino, R. J., Zellweger, G. W. and Bencala, K. E.: Retention and transport of nutrients in a third-order stream: channel processes, Ecology, 70(6), 1877–1892, doi:10.2307/1938119, 1989.

Vidon, P., Allan, C., Burns, D., Duval, T. P., Gurwick, N., Inamdar, S., Lowrance, R., Okay, J., Scott, D. and Sebestyen, S.: Hot spots and hot moments in riparian zones: Potential for improved water quality management, J. Am. Water Resour. Assoc., 46(2), 278–298, doi:10.1111/j.1752-1688.2010.00420.x, 2010.

Vidon, P. G. F. and Hill, A. R.: Landscape controls on nitrate removal in stream riparian zones, Water Resour. Res., 40(3), 1–14, doi:10.1029/2003WR002473, 2004.

Widdowson, M. A., Molz, F. J. and Benefield, L. D.: A numerical transport model for oxygen- and nitrate-based respiration linked to substrate and nutrient availability in porous media, Water Resour. Res., 24(9), 1553–1565, doi:10.1029/WR024i009p01553, 1988.

Wollschläger, U., Attinger, S., Borchardt, D., Brauns, M., Cuntz, M., Dietrich, P., Fleckenstein, J. H., Friese, K., Friesen, J., Harpke, A., Hildebrandt, A., Jäckel, G., Kamjunke, N., Knöller, K., Kögler, S., Kolditz, O., Krieg, R., Kumar, R., Lausch, A., Liess, M., Marx, A., Merz, R., Mueller, C., Musolff, A., Norf, H., Oswald, S. E., Rebmann, C., Reinstorf, F., Rode, M., Rink, K., Rinke, K., Samaniego, L., Vieweg, M., Vogel, H.-J., Weitere, M., Werban, U., Zink, M. and Zacharias, S.: The Bode hydrological observatory: a platform for integrated, interdisciplinary hydro-ecological research within the TERENO Harz/Central German Lowland Observatory, Environ. Earth Sci., 76(1), 29, doi:10.1007/s12665-016-6327-5, 2017.

Wondzell, S. M.: The role of the hyporheic zone across stream networks, Hydrol. Process., 25(22), 3525–3532, doi:10.1002/hyp.8119, 2011.

Zarnetske, J. P., Haggerty, R., Wondzell, S. M. and Baker, M. A.: Dynamics of nitrate production and removal as a function of residence time in the hyporheic zone, J. Geophys. Res., 116(G1), G01025, doi:10.1029/2010JG001356, 2011.

Zheng, L., Cardenas, M. B. and Wang, L.: Temperature effects on nitrogen cycling and nitrate removal-production efficiency in bed form-induced hyporheic zones, J. Geophys. Res. G Biogeosciences, 121(4), 1086–1103, doi:10.1002/2015JG003162, 2016.

Ziegel, E. R., Gibbons, J. and Chakraborti, S.: Nonparametric Statistical Inference, 5th ed., CRC Press, Boca Raton., 2011.